PHYSICAL REVIEW D **94,** 086006 (2016)

Efficiency of the Keplerian accretion in braneworld Kerr-Newman spacetimes and mining instability of some naked singularity spacetimes

Martin Blaschke[*] and Zdeněk Stuchlík[†]

Institute of Physics and Research Centre of Theoretical Physics and Astrophysics, Faculty of Philosophy and Science, Silesian University in Opava, Bezručovo náměstí 13, CZ-746 01 Opava, Czech Republic

(Received 1 August 2016; published 18 October 2016)

We show that the braneworld rotating Kerr-Newman black hole and naked singularity spacetimes with both positive and negative braneworld tidal charge parameters can be separated into 14 classes according to the properties of circular geodesics governing the Keplerian accretion. We determine the efficiency of the Keplerian accretion disks for all braneworld Kerr-Newman spacetimes. We demonstrate the occurrence of an infinitely deep gravitational potential in Kerr-Newman naked singularity spacetimes having the braneworld dimensionless tidal charge $b \in (1/4, 1)$ and the dimensionless spin $a \in (2\sqrt{b} - \sqrt{b(4b-1)}, 2\sqrt{b} + \sqrt{b(4b-1)})$, implying unbound efficiency of the Keplerian accretion and the possibility of extracting the whole naked singularity mass. Therefore, we call them braneworld "mining-unstable" Kerr-Newman naked singularity spacetimes. Fundamental restriction on the relevance of the extraordinary—but fully classical—phenomenon of the mining instability is given by validity of the assumption of geodesic motion of the accreting matter.

DOI: 10.1103/PhysRevD.94.086006

I. INTRODUCTION

In recent years, one of the most interesting and promising approaches to force-unification theory is represented by the higher-dimensional string theory and, in particular, M-theory [1,2]. In string theory and M-theory, gravity is described as a truly higher-dimensional interaction becoming effectively 4D at low enough energies. These theories inspired the so-called braneworld models, in which the observable Universe is a 3D-brane to which the standard particle-model fields are confined, while gravity enters the extra spatial dimensions [3]. The braneworld models provide an elegant solution to the hierarchy problem of the electroweak and quantum gravity scales, as these scales could become of the same order (in TeV) due to the large scale extra dimensions [3]. In fact, gravity can be localized near the D3-brane in the bulk space with a noncompact, infinite size extra dimension, with the warped spacetime satisfying the 5D Einstein equations [4]—the noncompact dimension can be related to M-theory. Future collider experiments can test the braneworld models quite well, including even the hypothetical mini–black hole production [5].

The 5D Einstein equations at the bulk space can be constrained to the 3D-brane, thus implying modified 4D Einstein equations [6]. Solution of these constrained 4D Einstein equations is quite complex in the presence of the matter stress-energy tensor, e.g., in the case of models of neutron stars [7–9]. However, it can be relatively simple in the case of vacuum solutions related to braneworld black holes. For both the spherically symmetric and static black holes that can be described by the Reissner-Nordström geometry [10] and the axially symmetric and stationary rotating black holes that can be described by the Kerr-Newman geometry [11], the influence due to the tidal effects from the bulk is simply represented by a single parameter. This parameter is called tidal charge because of the similarity of the effective stress-energy tensor of the tidal effects of the bulk space and the stress-energy tensor of the electromagnetic field [10].

The rotating braneworld black hole spacetimes and the related naked singularity spacetimes are thus represented by the Kerr-Newman geometry, but without the associated electromagnetic field occurring in standard general relativity [12]. The tidal charge parameter can be either positive or negative [10,11], while, in standard general relativity, only a positive parameter corresponding to the square of the electric charge occurs.

The standard studies of the Reissner-Nordström or Kerr-Newman black hole and naked singularity geodesic motion [13–17] can thus be directly applied for the braneworld black holes and naked singularities with positive tidal charge. The astrophysically relevant implications of the geodesic motion were extensively studied for the braneworld black holes (with both positive and negative tidal charges) in a number of papers related to the optical effects [18–25], or the test particle motion [26–33].

Here, we study the circular motion of test particles and photons in the braneworld Kerr-Newman spacetimes and give classification of the braneworld black hole and naked

[*]martin.blaschke@fpf.slu.cz
[†]zdenek.stuchlik@fpf.slu.cz

singularity spacetimes according to the properties of the radial profiles of specific angular momentum and specific energy of sequences of corotating and retrograde circular orbits. We give the classification for both the positive and negative values of the dimensionless tidal charge parameter. We also determine the efficiency of the Keplerian accretion disks that is related to the astrophysically relevant accretion from infinity (large distance) downwards to the first limit on existence of stable circular geodesics.

A very detailed analysis of the circular motion of electrically neutral test particles in the standard Kerr-Newman spacetimes was presented in [17], where both black hole and naked singularity spacetimes were discussed. The results of this study are relevant in the braneworld spacetimes with positive tidal charges; we do not repeat them, focusing our study on the phenomena related to the Keplerian accretion, its efficiency, and the phenomenon of a new special instability of the naked singularity spacetimes that were not considered in [17]. Along with the standard classical instability due to the Keplerian accretion occurring in the Kerr naked singularity spacetimes, leading to their conversion to a Kerr black hole [34–37], we have found a special class of classical instability, called here "mining" instability, as this instability is related to an unlimitedly deep gravitational potential well, occurring in the class of the Kerr-Newman naked singularity spacetimes with appropriately restricted values of their dimensionless spin a and dimensionless tidal charge b. We briefly discuss the limits on the applicability of the Keplerian accretion in relation to the mining instability.

II. BRANEWORLD KERR-NEWMAN GEOMETRY

Using the standard Boyer-Lindquist coordinates (t, r, θ, φ) and the geometric units ($c = G = 1$), we can write the line element of a rotating (Kerr-Newman) black hole or naked singularity, representing a solution of the Einstein equations constrained to the 3D-brane, in the form [10,11]

$$\begin{aligned} \mathrm{d}s^2 = &-\left(1-\frac{2Mr-b}{\Sigma}\right)\mathrm{d}t^2 - \frac{2a(2Mr-b)}{\Sigma}\sin^2\theta \mathrm{d}t\mathrm{d}\varphi \\ &+\frac{\Sigma}{\Delta}\mathrm{d}r^2 + \Sigma \mathrm{d}\theta^2 \\ &+\left(r^2+a^2+\frac{2Mr-b}{\Sigma}a^2\sin^2\theta\right)\sin^2\theta \mathrm{d}\varphi^2, \end{aligned} \tag{1}$$

where

$$\Delta = r^2 - 2Mr + a^2 + b, \tag{2}$$

$$\Sigma = r^2 + a^2\cos^2\theta. \tag{3}$$

M is the mass parameter of the spacetime, $a = J/M$ is the specific angular momentum of the spacetime with internal angular momentum J, and the braneworld parameter b, called the "tidal charge," represents an imprint of the nonlocal (tidal) gravitational effects of the bulk space [11].

The form of the metric (1) is the same as that of the standard Kerr-Newman solution of the 4D Einstein-Maxwell equations, with the squared electric charge Q^2 being replaced by the tidal charge b [12]. We can separate out three cases:

(a) $b = 0$, in which we are dealing with the standard Kerr metric.
(b) $b > 0$, in which we are dealing with the standard Kerr-Newman metric.
(c) $b < 0$, in which we are dealing with the nonstandard Kerr-Newman metric.

Notice that, in the braneworld Kerr-Newman spacetimes, the geodesic structure is relevant also for the motion of electrically charged particles, as there is no electric charge related to these spacetimes. On the other hand, case (b) can be equally considered for the analysis of the uncharged particle motion in the standard electrically charged Kerr-Newman spacetime.

For simplicity, we put in the following considerations $M = 1$. Then the spacetime parameters a and b and the time t and radial r coordinates become dimensionless. This is equivalent to the redefinition when we express all the quantities in units of M: $a/M \to a$, $b/M^2 \to b$, $t/M \to t$, and $r/M \to r$.

Separation between the black hole and naked singularity spacetimes is given by the relation of the spin and tidal charge parameters in the form

$$a^2 + b = 1, \tag{4}$$

determining the so-called extreme black hole with coinciding horizons. The condition $0 < a^2 + b < 1$ governs black hole spacetimes with two distinct event horizons, while the condition $a^2 + b < 0$ governs black hole spacetimes with only one distinct event horizon at $r > 0$. For $a^2 + b > 1$, the spacetime describes a naked singularity.

For positive tidal charges the black hole spin has to be $a^2 < 1$, as in the standard Kerr-Newman spacetimes, but, for negative tidal charges, there can exist black holes violating the well-known Kerr limit, having $a^2 > 1$ [28].

Using the substitutions

$$dt = dx^0 + \left(\frac{r^2+a^2}{\Delta} - 1\right)dr, \tag{5}$$

$$d\varphi = d\tilde{\varphi} + \frac{a}{\Delta}dr, \tag{6}$$

$$x = (r\cos(\tilde{\varphi}) + a\sin(\tilde{\varphi}))\sin\theta, \tag{7}$$

$$y = (r\sin(\tilde{\varphi}) - a\cos(\tilde{\varphi}))\sin\theta, \tag{8}$$

$$z = r\cos\theta, \tag{9}$$

the braneworld Kerr-Newman geometry can be transformed into the so-called Kerr-Schild form using the Cartesian coordinates:

$$ds^2 = -(dx^0)^2 + (dx)^2 + (dy)^2 + (dz)^2 + \frac{(2Mr-b)r^2}{r^4+a^2z^2}\left\{dx^0 - \frac{1}{r^2+a^2}\left[r(xdx+ydy) + a(xdy-ydx) - \frac{1}{r}zdz\right]\right\}^2, \tag{10}$$

where r is defined, implicitly, by

$$r^4 - r^2(x^2+y^2+z^2-a^2) - a^2z^2 = 0.$$

A. Singularity

The metric (10) is analytical everywhere except at points satisfying the condition

$$x^2+y^2+z^2 = a^2 \quad \text{and} \quad z = 0. \tag{11}$$

This condition is the same as in the case of the Kerr black holes or naked singularities, so we clearly see that the braneworld parameter b has no influence on the position of the physical singularity of the spacetime. The physical "ring" singularity of the braneworld rotating black holes (and naked singularities) is located at $r = 0$ and $\theta = \pi/2$, as in the Kerr spacetimes.

We describe the influence of the braneworld tidal charge parameter b on the Kerr-like ring singularity at $r = 0$, $\theta = \pi/2$ using the Kretschmann scalar $K = R_{\alpha\beta\gamma\delta}R^{\alpha\beta\gamma\delta}$, representing an appropriate tool to probe the structure of spacetime singularities. Using (1) we obtain

$$K = \frac{8}{(r^2+a^2y^2)^6}(r^4A - 2a^2r^2By^2 + a^4Cy^4 - 6a^6M^2y^6), \tag{12}$$

where

$$y = \cos\theta, \tag{13}$$

$$A = (7b^2 - 12bMr + 6M^2r^2), \tag{14}$$

$$B = (17b^2 - 60bMr + 45M^2r^2), \tag{15}$$

$$C = (7b^2 - 60bMr + 90M^2r^2). \tag{16}$$

The Kretschmann scalar is formally the same as in the case of the Kerr-Newman metric with $Q^2 \to b$ [38]. Naturally, the negative values of the brane parameter would have some effect on K, but, as we can see from the denominator of (12), it does not influence the location of the singularity. As an example we demonstrate the behavior of the scalar K for $a = 0.8$ and $b = -0.8$ near the ring singularity in Fig. 1.

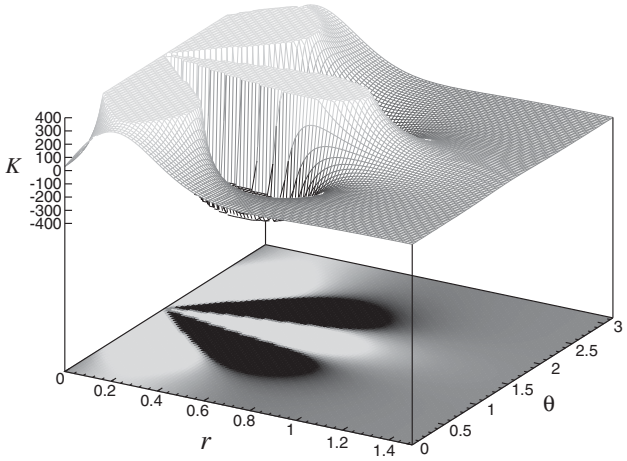

FIG. 1. Example of the behavior of the Kretschmann scalar K for $a = 0.8$ and $b = -0.8$ to illustrate its similarity to the Kerr-Newman case.

For completeness we also give the Ricci tensor whose components take the form

$$R_{tt} = 4b\frac{a^2+2\Delta-a^2\cos(2\theta)}{(a^2+2r^2+a^2\cos(2\theta))^3}, \tag{17}$$

$$R_{t\varphi} = -8ab\frac{(a^2+\Delta)\sin^2\theta}{(a^2+2r^2+a^2\cos(2\theta))^3}, \tag{18}$$

$$R_{\varphi t} = R_{t\varphi}, \qquad R_{rr} = -\frac{R_{\theta\theta}}{\Delta}, \tag{19}$$

$$R_{\theta\theta} = \frac{2b}{a^2+2r^2+a^2\cos(2\theta)}, \tag{20}$$

$$R_{\varphi\varphi} = 4b\sin^2(\theta)\frac{3a^4+2r^4+a^2(b-2Mr+5r^2)}{(a^2+2r^2+a^2\cos(2\theta))^3} - \frac{a^2\Delta\cos(2\theta)}{(a^2+2r^2+a^2\cos(2\theta))^3}. \tag{21, 22}$$

Ricci scalar is automatically zero by construction of the braneworld Kerr-Newman solution [10].

B. Ergosphere

Here, we demonstrate the influence of the braneworld tidal charge parameter b on the ergosphere whose boundary is defined by the condition

$$g_{tt} = r^2 - 2Mr + a^2\cos^2\theta + b = 0. \tag{23}$$

Extension of the ergosphere in the latitudinal coordinate θ is determined by the maximal latitude given by the relation

$$\cos^2\theta_{\max} = \frac{1-b}{a^2}. \tag{24}$$

We can see that the existence of the ergosphere is limited by the condition

$$b < 1. \tag{25}$$

We can infer that the ergosphere extension increases as the tidal charge parameter b decreases.

It is convenient to represent location of the ergosphere in the Kerr-Schild coordinates (10). Using the spacetime symmetry, we can focus only on the polar slices with $y = 0$. In this case the condition for the static limit surface governing the border of the ergosphere is simply given by [39]

$$x^2 = \frac{(a^2+r^2)\Delta}{a^2},$$
$$z^2 = \frac{(2r-b)r^2 - r^4}{a^2}. \tag{26}$$

In Fig. 2 we illustrate the influence of the braneworld tidal charge b on the ergosphere extension.

The ergosphere does not always completely surround the ring singularity. To illustrate this phenomenon, we also give the dependence of the maximal allowed latitudinal angle of the ergosphere on the dimensionless spin and dimensionless tidal charge.

For $b < 1$, the ergosphere exists for each dimensionless spin $a > 0$, covering all values of the latitudinal angle for the Kerr-Newman black holes. However, as the spin a increases for the Kerr-Newman naked singularities, the ergosphere extension shrinks—the maximal angle α decreases.

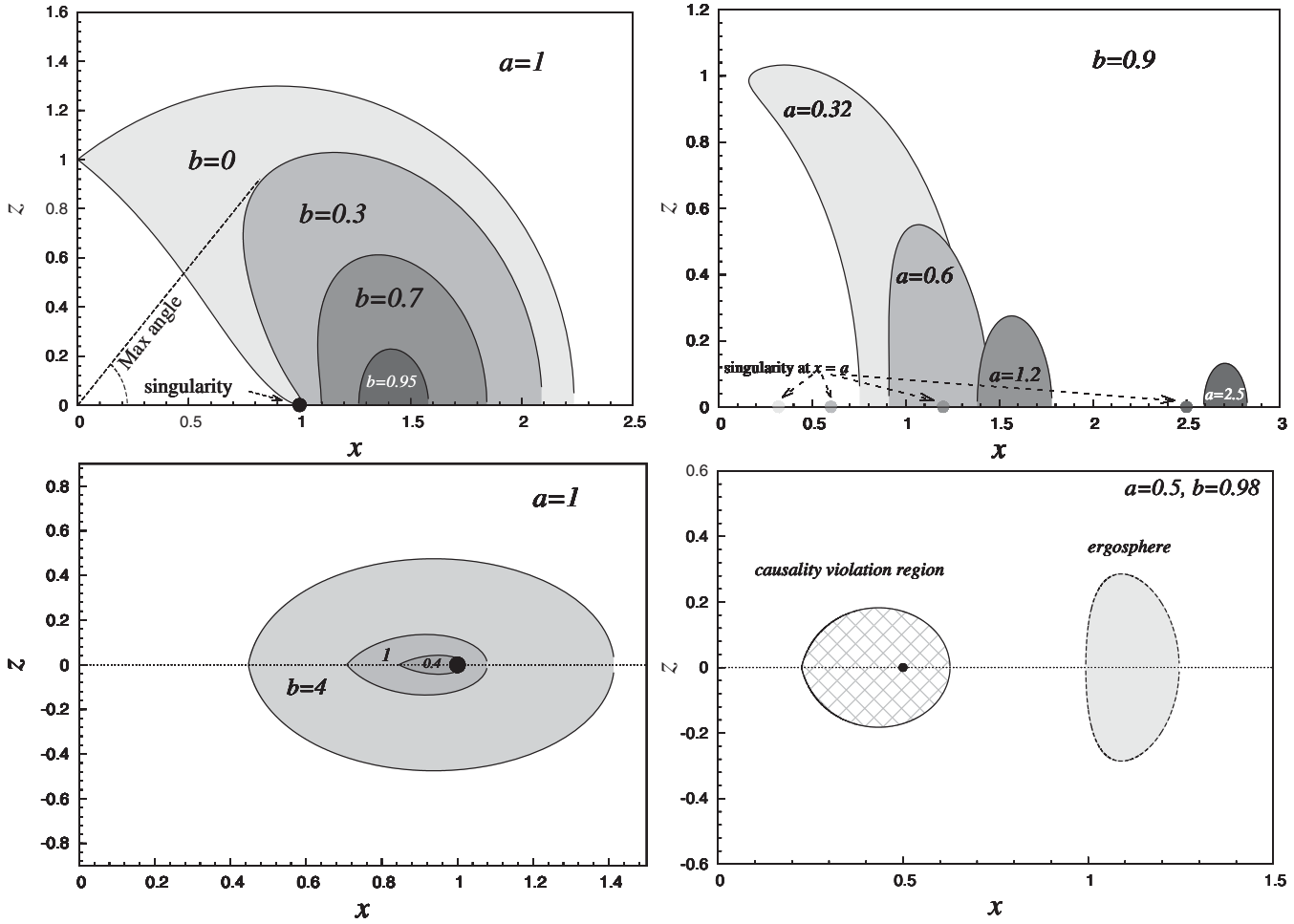

FIG. 2. (Upper left panel) Polar slice through the braneworld Kerr-Newman spacetime in the Cartesian Kerr-Schild coordinates. The dimensionless spin parameter a is fixed at 1 and the braneworld parameter b is appropriately chosen to demonstrate its influence on the ergosphere. (Upper right panel) Polar slice through the braneworld Kerr-Newman spacetime in the Cartesian Kerr-Schild coordinates. The braneworld parameter b is fixed at 0.9 and the spin parameter a is appropriately chosen to demonstrate its influence on the ergosphere. (Lower left panel) Causality violation region. (Lower right panel) Ergosphere and causality violation region.

C. Causality violation region

In the "causality violation region" (sometimes called the time-machine region), the axial coordinate φ takes timelike character, implying the possible existence of closed timelike curves. The causality violation region is defined by the condition

$$g_{\varphi\varphi} < 0. \tag{27}$$

In the equatorial plane, the boundary of the causality violation region is determined by the condition

$$r^4 + a^2(r^2 + 2r - b) = 0. \tag{28}$$

The boundary of the causality violation region can be expressed by the relation

$$b = b_{\rm CV} \equiv \frac{r(2a^2 + a^2 r + r^3)}{a^2}. \tag{29}$$

In Fig. 3 we give some examples of the extension of the causality violation region. We see that, for this region to exist above the ring singularity, the tidal charge has to be positive. With increasing values of the parameters $b > 0$ and a, the causality violation region expands.

Equation (28) gives us maximal possible extension of the causal violation region located at

$$r_{\rm Max} = \sqrt{1 + b} - 1. \tag{30}$$

For a positive b, the value of $r_{\rm Max}$ is less than b and therefore, as we shall see later, the causality violation region cannot reach the region where the circular geodesics exist.

In the Kerr-Schild coordinates, the boundary of the causality violation region is given by the relations

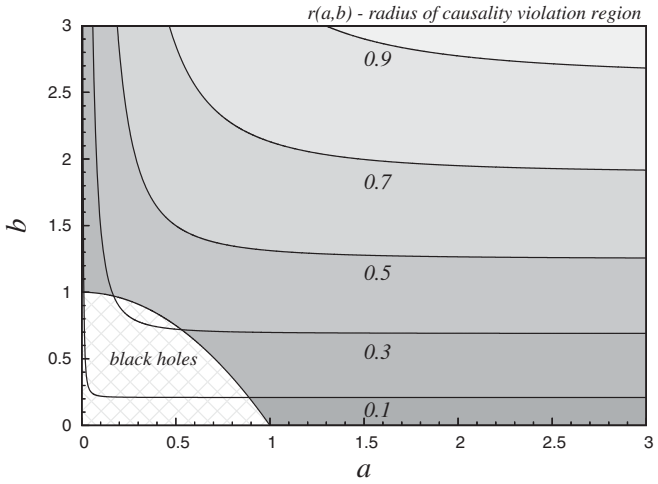

FIG. 3. Contour plot for radii of the boundary of the causality violation region in the equatorial plane.

$$x^2 = \frac{(a^2 + r^2)^3}{a^2\Delta}, \tag{31}$$

$$z^2 = \frac{r^2(a^2(b - 2r - r^2) - r^4)}{a^2\Delta}. \tag{32}$$

It can be proved that the causality violation region never overlaps with the ergosphere, and its extension is influenced by the braneworld parameter b in the opposite way. While causality violation region increases with an increasing b, the ergosphere extension gets smaller. This phenomenon is illustrated in Fig. 2, where the Kerr-Schild coordinates are used.

In the following, we consider geodesic motion only in the regions above the causality violation region. For astrophysical phenomena occurring in the naked singularity spacetimes, it is usually assumed that, above the boundary of the causality violation region, the Kerr or Kerr-Newman spacetime is removed and substituted for a different solution that could be inspired by string theory—such objects are called superspinars [40–42]. Therefore, it is quite natural to assume that, in the braneworld model framework, the inner boundary of the superspinars is located at radii larger than those related to the boundary of the causality violation region.

D. Locally nonrotating frames

In the rotating Kerr-Newman spacetimes, physical processes can be most conveniently expressed in the family of locally nonrotating frames (LNRFs), corresponding to zero angular momentum observers, with tetrad vectors given by the relations [43]

$$\mathbf{e}^{(t)} = (\omega^2 g_{\varphi\varphi} - g_{tt})^{\frac{1}{2}}\mathbf{d}t, \tag{33}$$

$$\mathbf{e}^{(\varphi)} = (g_{\varphi\varphi})^{\frac{1}{2}}(\mathbf{d}\varphi - \omega\mathbf{d}t), \tag{34}$$

$$\mathbf{e}^{(r)} = \left(\frac{\Sigma}{\Delta}\right)^{\frac{1}{2}}\mathbf{d}r, \tag{35}$$

$$\mathbf{e}^{(\theta)} = \Sigma^{\frac{1}{2}}\mathbf{d}\theta, \tag{36}$$

where ω is the angular velocity of the LNRFs relative to distant observers and reads

$$\omega = -\frac{g_{t\varphi}}{g_{\varphi\varphi}} = \frac{a(2r - b)}{\Sigma(r^2 + a^2) + (2r - b)a^2\sin^2\theta}. \tag{37}$$

Convenience of the LNRFs can be demonstrated, e.g., in the case of the free fall of particles from infinity, which is purely radial only if related to the family of the LNRFs [44].

E. Geodesic motion and Carter's equations

Using the Hamilton-Jacobi method, Carter found separated first order differential equations of the geodesic motion [39,45], which in the case of the braneworld Kerr spacetimes take the form

$$\Sigma\frac{\mathrm{d}r}{\mathrm{d}w}=\pm\sqrt{R(r)}, \tag{38}$$

$$\Sigma\frac{\mathrm{d}\theta}{\mathrm{d}w}=\pm\sqrt{W(\theta)}, \tag{39}$$

$$\Sigma\frac{\mathrm{d}\varphi}{\mathrm{d}w}=-\frac{P_W}{\sin^2\theta}+\frac{aP_R}{\Delta}, \tag{40}$$

$$\Sigma\frac{\mathrm{d}t}{\mathrm{d}w}=-aP_W+\frac{(r^2+a^2)P_R}{\Delta}, \tag{41}$$

where

$$R(r)=P_R^2-\Delta(m^2r^2+\tilde{K}), \tag{42}$$

$$W(\theta)=(\tilde{K}-a^2m^2\cos^2\theta)-\left(\frac{P_w}{\sin\theta}\right)^2, \tag{43}$$

$$P_R(r)=\tilde{E}(r^2+a^2)-a\tilde{\Phi}, \tag{44}$$

$$P_W(\theta)=a\tilde{E}\sin^2\theta-\tilde{\Phi}. \tag{45}$$

Along with the conservative rest energy m, three constants of motion related to the spacetime symmetries have been introduced: $\tilde{E}$ is the energy (related to the time Killing vector field), $\tilde{\Phi}$ is the axial angular momentum (related to the axial Killing vector field), and $\tilde{K}$ is the constant of motion related to the total angular momentum (related to the Killing tensor field) that is usually replaced by the constant $\tilde{Q}=\tilde{K}-(a\tilde{E}-\tilde{\Phi})^2$ since, for the motion in the equatorial plane ($\theta=\pi/2$), we have $\tilde{Q}=0$.

Note that the separable Eqs. (38)–(41) are quaranteed in the Petrov type D spacetimes, particularly when the metric in the Boyer-Lindquist coordinates can be expressed in the Kerr-like form by replacing the mass parameter M by a function $M(r)$ independent of latitude θ. In the braneworld rotating black hole spacetimes, we have $M(r)=M-\frac{b}{2r}$. Generally, these equations can be integrated and expressed in terms of the hyperelliptic integrals [12,46,47]. The Carter equations can also be generalized to the motion in the Kerr-Newman–de Sitter spacetimes [39,46,48–50].

For the geodesic motion of photons, we put $m=0$ in the Carter equations. Analysis of the photon motion in the standard Kerr-Newman spacetimes [17,51,52] can be directly applied to the case of photon motion in the braneworld Kerr-Newman spacetimes. This has been done in [19]; we use the results of these works in the following discussions.

We have to construct classification of the braneworld Kerr-Newman spacetimes according to the properties of circular geodesics governing the Keplerian accretion, which can be related not only to the standard accretion disks but also to the quasicircular motion of gravitationally radiating particles. We give classifications according to the properties of the circular null geodesics and the stability of the circular geodesics that become the critical attribute of the Keplerian accretion. Finally, we combine the effects given by these two classifications. Of course, we have to also include in the classification as relevant criteria the existence of the event horizons and the existence of the ergosphere.

III. CIRCULAR GEODESIC MOTION

In general stationary and axially symmetric spacetime with the Boyer-Lindquist coordinate system (t,r,θ,φ) and the $(-+++)$ signature of the metric tensor, the line element is given by

$$ds^2=g_{tt}dt^2+2g_{t\varphi}dtd\varphi+g_{rr}dr^2+g_{\theta\theta}d\theta^2+g_{\varphi\varphi}d\varphi^2. \tag{46}$$

The metric (46) is adapted to the symmetries of the spacetime, endowed with the Killing vectors $(\partial/\partial t)$ and $(\partial/\partial\varphi)$ for time translations and spatial rotations, respectively. For geodesic motion in the equatorial plane ($\theta=\pi/2$), the metric functions g_{tt}, $g_{t\varphi}$, g_{rr}, $g_{\theta\theta}$, and $g_{\varphi\varphi}$ in Eq. (46) depend only on the radial coordinate r. Thus, omitting the rest energy m, two integrals of the motion are relevant when $\tilde{Q}=0$:

$$U_t=-E, \qquad U_\varphi=L, \tag{47}$$

where the 4-velocity $U_\alpha=g_{\alpha\nu}dx^\nu/d\tau$, with τ being the affine parameter. In the case with an asymptotically flat spacetime, we can identify at infinity the motion constant $E=\tilde{E}/m$ as the specific energy, i.e., energy related to the rest energy, and the motion constant $L=\tilde{\Phi}/m$ as the specific angular momentum.

The geodesic equations of the equatorial motion take the form (see, e.g., [53])

$$\frac{dt}{d\tau}=\frac{Eg_{\varphi\varphi}+Lg_{t\varphi}}{g_{t\varphi}^2-g_{tt}g_{\varphi\varphi}}, \qquad \frac{d\varphi}{d\tau}=-\frac{Eg_{t\varphi}+Lg_{tt}}{g_{t\varphi}^2-g_{tt}g_{\varphi\varphi}}, \tag{48}$$

and

$$g_{rr}\left(\frac{dr}{d\tau}\right)^2=R(r), \tag{49}$$

where the radial function $R(r)$ is defined by

$$R(r) \equiv -1 + \frac{E^2 g_{\varphi\varphi} + 2EL g_{t\varphi} + L^2 g_{tt}}{g_{t\varphi}^2 - g_{tt} g_{\varphi\varphi}}. \quad (50)$$

A. Energy, angular momentum, and angular velocity of circular geodesics

For circular geodesics in the equatorial plane, the conditions

$$R(r) = 0 \quad \text{and} \quad \partial_r R(r) = 0 \quad (51)$$

must be satisfied simultaneously. These conditions determine the specific energy E, the specific angular momentum L and the angular velocity $\Omega = d\varphi/dt$ related to distant observers, for test particles following the circular geodesics, as functions of the radius and the spacetime parameters in the form

$$E = \pm \frac{g_{tt} + g_{t\varphi}\Omega}{\sqrt{-(g_{tt} + 2g_{t\varphi}\Omega + g_{\varphi\varphi}\Omega^2)}}, \quad (52)$$

$$L = \mp \frac{g_{t\varphi} + g_{\varphi\varphi}\Omega}{\sqrt{-(g_{tt} + 2g_{t\varphi}\Omega + g_{\varphi\varphi}\Omega^2)}}, \quad (53)$$

$$\Omega = \frac{-g_{t\varphi,r} \pm \sqrt{(g_{t\varphi,r})^2 - g_{tt,r} g_{\varphi\varphi,r}}}{g_{\varphi\varphi,r}}, \quad (54)$$

where the upper and lower signs refer to two families of solutions. To avoid any misunderstanding, we will refer to these two families as the upper sign family and the lower sign family. At large distances in the asymptotically flat spacetimes, the upper family orbits are corotating, while the lower family orbits are counterrotating with respect to the rotation of the spacetime. This separation holds in the whole region above the event horizon of the Kerr-Newman black hole spacetimes, but this is not necessarily so in all of the Kerr-Newman naked singularity spacetimes—in some of them the upper family orbits become counterrotating close to the naked singularity, as demonstrated in [35].

Using the spacetime line element of the braneworld rotating spacetimes given by (1) [11,54] and assuming that $M = 1$, we obtain the radial profiles of the specific energy, the specific axial angular momentum, and the angular velocity related to infinity of the circular geodesics in the form

$$E = \frac{r^2 - 2r + b \pm a\sqrt{r-b}}{r\sqrt{r^2 - 3r + 2b \pm 2a\sqrt{r-b}}}, \quad (55)$$

$$L = \pm \frac{\sqrt{r-b}(r^2 + a^2 \mp 2a\sqrt{r-b}) \mp ab}{r\sqrt{r^2 - 3r + 2b \pm 2a\sqrt{r-b}}}, \quad (56)$$

$$\Omega = \pm \frac{1}{\frac{r^2}{\sqrt{r-b}} \pm a}. \quad (57)$$

From Eqs. (55)–(57) we immediately see that two restrictions on the existence of circular geodesics have to be satisfied:

$$r^2 - 3r + 2b \pm 2a\sqrt{r-b} \geq 0, \quad (58)$$

$$r \geq b. \quad (59)$$

The equality in the first condition determines the photon circular geodesics—this demonstrates that positions of circular orbits of test particles are limited by the circular geodesics of massless particles. The second reality condition is relevant in the Kerr-Newman spacetimes with the positive tidal charge b only if we restrict our attention to the region of positive radii.

B. Effective potential

Instead of the radial function $R(r, a, b, E, L)$, the equatorial motion of test particles can be conveniently treated by using the so-called effective potential $V_{\rm Eff}(r, a, b, L)$, which is related to the particle specific energy and depends on the specific angular momentum of the motion and the spacetime parameters. The equation $E = V_{\rm Eff}$ determines the turning points of the radial motion of the test particle.

The notion of the effective potential is useful in treating the Keplerian (quasigeodesic) accretion onto the central object that is directly related to the circular geodesic motion [55,56]. The circular geodesics are governed by the local extrema of the effective potential; the accretion process is possible in the regions of stable circular geodesics corresponding to the local minima of the effective potential.

The effective potential can be easily derived using the normalization condition for the test particle motion

$$U_\alpha U^\alpha = -1, \quad (60)$$

which implies, for the equatorial motion relation,

$$g_{rr}\left(\frac{dr}{d\tau}\right)^2 = (E - V_{\rm Eff+})(E - V_{\rm Eff-}), \quad (61)$$

and, in the general stationary and axisymmetric spacetimes, the effective potential can be expressed in the form

$$V_{\rm Eff\pm}(r, a, b, L) = \frac{\beta \pm \sqrt{\beta^2 - \alpha\gamma}}{\alpha}, \quad (62)$$

where

$$\alpha = \frac{g_{\varphi\varphi}}{g_{\varphi t}^2 - g_{\varphi\varphi} g_{tt}}, \qquad \beta = \frac{-L g_{t\varphi}}{g_{\varphi t}^2 - g_{\varphi\varphi} g_{tt}}, \quad (63)$$

$$\gamma = \frac{L^2 g_{tt}}{g_{\varphi t}^2 - g_{\varphi\varphi} g_{tt}} - 1. \tag{64}$$

This form can be simplified to

$$V_{\mathrm{Eff}\pm} = \frac{-L g_{t\varphi} \pm \sqrt{(L^2 + g_{\varphi\varphi})(g_{t\varphi}^2 - g_{\varphi\varphi} g_{tt})}}{g_{\varphi\varphi}}. \tag{65}$$

We have to choose the upper (plus) sign of the general expression of the effective potential, as this case represents the boundary of the motion of particles in the so-called positive-root states having a positive locally measured energy and a future-oriented time component of the 4-velocity. The lower (minus) sign expression of the effective potential is irrelevant here, as it determines in the regions of interest particles in the so-called negative-root states having a negative locally measured energy and a past-oriented time component of the 4-velocity, thus being related to the Dirac particles—for details, see [12,57].

The physically relevant condition of the test particle motion reads

$$E \geq V_{\mathrm{Eff}+}. \tag{66}$$

For particles with the nonzero rest mass, $m > 0$, the explicit form of the effective potential in the braneworld Kerr-Newman spacetimes reads

$$V_{\mathrm{Eff}}(r, a, b, L) = \frac{aL(2r - b) + r\sqrt{\Delta}\sqrt{L^2 r^2 + r^4 + a^2(r^2 + 2r - b)}}{r^4 + a^2(r^2 + 2r - b)}. \tag{67}$$

For massless particles, $m = 0$, we formally obtain

$$\frac{V_{\mathrm{Effp}}(r, a, b)}{L} = \frac{a(2r - b) \pm r^2\sqrt{\Delta}}{r^4 + a^2(r^2 + 2r - b)}. \tag{68}$$

Here, the plus sign is valid if $L > 0$ and the minus sign is valid if $L < 0$. Of course, we know that the photon geodesic motion is independent of the photon energy, being dependent on the impact parameter $l = L/E$ for the equatorial motion [41,58].

The effective potential is symmetric under the transformation $a \to -a$, $L \to -L$; therefore, we will only study the Kerr-Newman braneworld spacetimes with nonnegative values of the spin parameter a.

The effective potential has a discontinuity (divergence) at radii determined by the conditions

$$g_{\varphi t}^2 - g_{\varphi\varphi} g_{tt} = 0, \tag{69}$$

$$r^4 + a^2(r^2 + 2r - b) = 0. \tag{70}$$

At the equatorial plane, the quantity $g_{\varphi t}^2 - g_{\varphi\varphi} g_{tt} \equiv \Delta$, and the condition (69) implies that the effective potential diverges at the event horizons. The second condition (70) for a possible divergence of the effective potential can be transformed to the relation

$$b = b_{\mathrm{s}} \equiv \frac{r(2a^2 + a^2 r + r^3)}{a^2}. \tag{71}$$

Notice that the functions $b_{\mathrm{s}}(r, a)$ and $b_{\mathrm{CV}}(r, a)$ are equivalent—therefore, the divergence could occur just at the boundary of the causality violation region. In the limit of $b \to b_S$, the numerator of (67) reads

$$-\frac{r}{a}(L - |L|)(a^2 + r^3). \tag{72}$$

Thus, if $L \geq 0$, both the numerator and the denominator of (67) are zero and we have to use the L'Hôpital rule to obtain

$$\lim_{b \to b_{\mathrm{s}}} V_{\mathrm{Eff}} = \begin{cases} \frac{r^4 + a^4 + 2a^2(L^2 + r^2) + L^2 r^2}{2aL(a^2 + r^2)} & L \geq 0 \\ \infty & L < 0 \end{cases}. \tag{73}$$

Therefore, for the specific angular momentum $L < 0$, the effective potential approaches at the discontinuity positive infinity, thus creating an impenetrable barrier for the test particles with $L < 0$. On the other hand, for particles with $L \geq 0$, the effective potential takes, at the boundary of the causality violation region, a finite value that depends on the specific angular momentum.

The last square root in Eq. (67) is negative for

$$b > \frac{r(2a^2 + a^2 r + L^2 r + r^3)}{a^2}. \tag{74}$$

Therefore, the effective potential can be undefined for small values of r. However, this could happen only in the causality violation region, where the effective potential looses its relevance because of the modified meaning of the axial coordinate that has a timelike character in this region.

C. Energy measured in LNRFs

It is useful to determine, for particles on the circular geodesics, the locally measured energy related to some properly defined family of observers. The specific energy related to the LNRF (E_{LNRF}) is given by the projection of the 4-velocity on the timelike vector of the frame:

$$E_{\mathrm{LNRF}} = U^{(t)} = U^{\mu} \mathbf{e}_{\mu}^{(t)} = \left(\frac{dt}{d\tau}\right) \mathbf{e}_t^{(t)} = \frac{r^2 \pm a\sqrt{r - b}}{\sqrt{r^4 + a^2(r^2 + 2r - b)}} \times \frac{\sqrt{\Delta}}{\sqrt{r^2 - 3r + 2b \pm 2a\sqrt{r - b}}}. \tag{75}$$

The locally measured particle energy must always be positive for the particles in the positive-root states assumed

here, while it is negative for the negative-root states that are physically irrelevant in the context of our study [57].

The LNRF energy of the particle following the circular geodesics diverges on the photon circular orbit as well as the covariant energy E. It also diverges for circular orbits approaching the boundary of the causality violation region given by Eq. (70).

D. Future-oriented particle motion

For the positive-root states, the time evolution vector has to be oriented to the future, i.e., $dt/d\tau > 0$. On the other hand, the negative-root states have past-oriented time vectors, $dt/d\tau < 0$, and thus are physically irrelevant for our study. To be sure that we are using the solutions related to the proper effective potential $V_{\rm eff}$ with the correct upper sign, we have to ensure that the considered geodesics have the proper orientation, $dt/d\tau > 0$.

Using the metric (1) and relations for the specific energy (55) and specific angular momentum (56) in Eq. (48), we obtain the time component of the 4-velocity for both the upper and lower family circular geodesics in the form

$$\frac{dt}{d\tau} = \frac{r^2 \pm a\sqrt{r-b}}{r\sqrt{r^2 - 3Mr + 2b \pm 2a\sqrt{Mr-b}}}. \tag{76}$$

We see from this equation that the time component is always positive for the orbits of both the upper and the lower family, so we always have the positive-root states, and no mixing with the negative-root states occurs.

IV. CIRCULAR GEODESICS OF PHOTONS

We first study motion of photons, as the photon circular orbits represent a natural boundary for the existence of circular geodesic motion [52,58].

The general photon motion in the braneworld Kerr-Newman black hole spacetimes was studied in [19]. Here, we concentrate on the equatorial photon motion and, especially, on the existence of the photon circular orbits. In the case of the equatorial photon orbits, the radial function $R(r)$ is determined by Eq. (50) with the removed term -1 (with the rest energy $m = 0$), which can be transformed into the form [19]

$$\frac{R}{E^2} = \frac{[r^2 - a(\lambda - a)]^2 - \Delta(\lambda - a)^2}{r^2\Delta}, \tag{77}$$

where the impact parameter λ is defined by the relation

$$\lambda = \frac{L}{E}. \tag{78}$$

Notice that the photon orbits depend only on the impact parameter λ.

Applying conditions for the circular motion (51), we find that the equatorial photon circular orbits are given by the equations

$$[r^2 - a(\lambda - a)]^2 - \Delta(\lambda - a)^2 = 0, \tag{79}$$

$$2r(r^2 + a^2 - a\lambda) - (r-1)(\lambda - a)^2 = 0. \tag{80}$$

These two conditions imply that the radii of the circular photon orbits are determined by the equation

$$r^2 - 3r + 2a^2 + 2b \pm 2a\sqrt{\Delta} = 0, \tag{81}$$

and the impact parameter λ is given by the equation

$$\lambda = -a\frac{r^2 + 3r - 2b}{r^2 - 3r + 2b}. \tag{82}$$

Furthermore, Eq. (81) can by transformed into the form

$$r^2 - 3r + 2b \pm 2a\sqrt{r-b} = 0, \tag{83}$$

which implies the same reality condition on the radius of the photon orbit $r_{\rm ph}$ as the one that follows from Eqs. (55)–(57):

$$r_{\rm ph} \geq b. \tag{84}$$

Because of the reality condition, the numerator in Eq. (82) is positive, while the $(\pm)$ in the denominator is determined by the sign in Eq. (83). Thus, we obtain corotating orbits ($\lambda > 0$) for the upper sign in (83), and counterrotating orbits ($\lambda < 0$) in the other case.

The solution of Eq. (83) can be expressed in the form

$$a = a_{\rm ph}(r,b) \equiv \pm\frac{(3r - r^2 - 2b)}{2\sqrt{r-b}}. \tag{85}$$

For a given a and b, the points of a line $a = \text{const}$ crossing the function $a_{\rm ph}(r,b)$ determine the radius, $r_{\rm ph}$, of the photon circular orbits. We restrict our discussion to the solutions corresponding to $a > 0$, giving both corotating and counterrotating orbits. The zeros of the function $a_{\rm ph}(r,b)$ are located at

$$r_{\rm ph\pm} = \frac{1}{2}(3 \pm \sqrt{9 - 8b}). \tag{86}$$

Note that these solutions represent radii of photon circular orbits in the Reissner-Nordström spacetimes [15,16]. Since

$$\frac{\partial a_{\rm ph}}{\partial r} = \pm\frac{(r-1)(3r-4b)}{4(r-b)^{3/2}}, \tag{87}$$

the extrema of the curves $a_{\rm ph}(r,b)$ are located at $r = 1$ and at $r = 4b/3$. The value of the function $a_{\rm ph}(r,b)$ at the point $r = 1$ reads (recall that we consider the positive values of the spin)

$$a_{\text{ph-ex}}(r = 1, b) = \sqrt{1-b}, \tag{88}$$

TABLE I. All kinds of extrema of the function $a_{\rm ph}(r,b)$. We show the plus sign part only because of the symmetry corresponding to the interchangeability between signs ($\pm$) and the nature of the local minima (max/min). The function $a_{\rm phMin}$ is the value of the function $a_{\rm ph}(r,b)$ at the lowest possible r, which is $r=0$ for nonpositive values of b and $r=b$ otherwise.

r	b						
	$(-\infty;0)$	$(0;\frac{3}{4})$	$(\frac{3}{4};1)$	1	$(1;\frac{9}{8})$	$(\frac{9}{8};\infty)$	$a_{\rm ph}(r,b)$
1	max	max	min	$\cdots$	$\cdots$	$\cdots$	$\sqrt{1-b}$
r_1, r_2	min	min	min	min	min	$\cdots$	0
$\frac{4}{3}b$	$\cdots$	min	max	max	max	min	$\frac{\sqrt{b}}{3\sqrt{3}}(8b-9)$
$a_{\rm phMin}$	$-b$	∞	∞	0	∞	∞	$\cdots$

corresponding to the extreme Kerr-Newman black holes, while, at $r=4b/3$, it reads

$$a_{\text{ph-ex}}(r=4b/3,b)=\pm\frac{\sqrt{b}}{3\sqrt{3}}(8b-9). \tag{89}$$

The position, value, and kind of the extrema of the function $a_{\rm ph}(r,b)$ are listed in Table I. The results are summarized in Fig. 4. We see that all curves drawn there—the curve $a_{\text{ph-ex}}(r=4b/3,b)$, the line $a^2+b=1$ (corresponding to the extremal black holes), the line $a^2+b=0$, and the line $b=1$ (separating the braneworld Kerr-Newman naked singularities with the ergosphere from those without it)—divide the b-a plane into ten regions. In this sense, the braneworld Kerr-Newman spacetimes can be divided into ten different classes, characterized by

(1) existence of the horizon,
(2) existence of the ergosphere, and
(3) the number of stable and unstable circular photon orbits.

The situation is summarized in Table II and is also depicted in Fig. 4, in accord with the analysis of circular photon orbits in the standard Kerr-Newman spacetimes [52]. In the case of the braneworld Kerr-Newman black holes, the new regions VIII, IX, and X corresponding to the negative values of the tidal charge, ($b<0$), occur in addition to the standard Kerr-Newman spacetimes.

TABLE II. Ten possible divisions of braneworld Kerr-Newman spacetimes with respect to the existence of the horizon, the existence of the ergosphere, and the number of stable and unstable circular photon orbits. The first number in the column orbits corresponds to the amount of stable circular photon orbits, while the second corresponds to the amount of unstable circular photon orbits.

Class	Horiz.	Ergo.	Orbits	Class	Horiz.	Ergo.	Orbits
I	yes	yes	0, 2	VI	no	yes	2, 2
II	yes	yes	1, 3	VII	no	no	2, 2
III	no	yes	1, 1	VIII	yes	yes	0, 2
IV	no	no	1, 1	IX	yes	yes	0, 3
V	no	no	0, 0	X	no	yes	0, 1

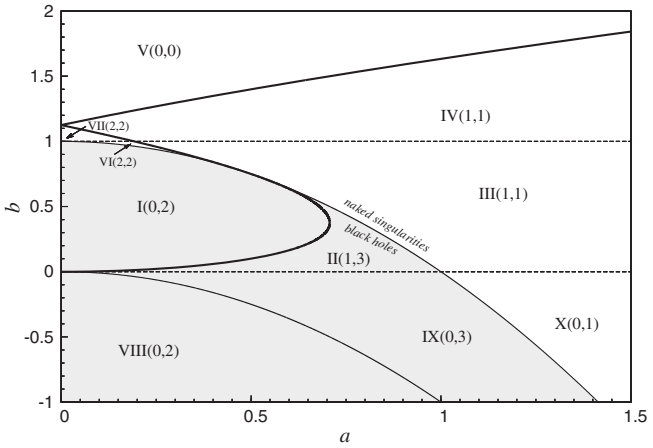

FIG. 4. Braneworld Kerr-Newman black holes and naked singularities can be divided into ten distinguish classes according to the properties of the circular photon geodesics. Curve $a_{\rm ph}(4b/3,b)$ (the solid line), given by (88), plays the main role in the classification. The corresponding regions of the b-a plane are denoted by I–X; the numbers in brackets denote the number of circular photon orbits in the respective classes. The first number determines the number of stable circular photon geodesics, while the second number determines the number of unstable circular photon geodesics.

V. STABLE CIRCULAR GEODESICS

It is well known that the character of the test particle (geodesic) circular motion governs the structure of the Keplerian (geometrically thin) accretion disks orbiting a black hole [55,56] or a naked singularity (superspinar) [36,37]; similarly, it can also govern the motion of a satellite orbiting the black hole or the naked singularity (superspinar) along a quasicircular orbit slowly descending due to the gravitational radiation of the orbiting satellite [59]. The Keplerian accretion, starting at large distances from the attractor, is possible in the regions of the black hole or naked singularity spacetimes where local minima of the effective potential exist, and the energy corresponding to these minima decreases with decreasing angular momentum [12]. In other words, in terms of the radial profiles of the quantities characterizing circular geodesics, the Keplerian accretion is possible where both specific angular momentum and the specific energy of the circular geodesics decrease with a decreasing radius. In the standard model of the black hole accretion disks, the inner edge of the accretion disk is located in the so-called marginally stable circular geodesic where the effective potential has an inflection point [55], but the situation can be more complex in the naked singularity spacetimes [15,60].

We study the stability of the circular geodesic motion of the test particles relative to the radial perturbations in the braneworld Kerr-Newman spacetimes. Note that the

equatorial circular motion is then always stable relative to the latitudinal perturbations perpendicular to the equatorial plane [61]. We show that the most interesting and, in fact, an unexpected result occurs for test particles orbiting the special class of the braneworld mining-unstable Kerr-Newman naked singularities, demonstrating an infinitely deep gravitational well enabling (formally) unlimited energy mining from the naked singularity spacetime. Of course, such a mining must be limited by a violation of the assumption of the test particle motion.

A. Marginally stable circular geodesics

The loci of the stable circular orbits are given by the condition related to the radial motion $R(r)$ function

$$\frac{\partial^2 R(r,a,b,E,L)}{\partial r^2} \leq 0, \tag{90}$$

or the relation

$$\frac{\partial^2 V_{\rm Eff}(r,a,b,L)}{\partial r^2} \leq 0, \tag{91}$$

related to the effective potential $V_{\rm Eff}(r)$, where the case of equality corresponds to the marginally stable circular orbits at $r_{\rm ms}$ with $L = L_{\rm ms}$, corresponding to the inflection point of the effective potential—for lower values of the specific angular momentum L, the particle cannot follow a circular orbit. Such a marginally stable circular orbit represents the innermost stable circular orbit and the inner edge of the Keplerian disks in the Kerr black hole and in naked singularity spacetimes.

Using the relations (55) and (56), we obtain for the braneworld Kerr-Newman spacetimes [28,62]

$$r(6r - r^2 - 9b + 3a^2) + 4b(b - a^2) \mp 8a(r-b)^{3/2} = 0. \tag{92}$$

In the previous studies, only the braneworld black hole spacetimes were typically considered [27,28]. Standard Kerr-Newman naked singularity spacetimes were discussed in [17,57]. Here, we consider the whole family of the braneworld Kerr-Newman spacetimes, with both positive and negative tidal charges. The solution of Eq. (92) can be expressed in the form

$$a_{\rm ms} = \mp \frac{4(r-b)^{3/2} \pm \sqrt{3br^2 - (2+4b)r^3 + 3r^4}}{4b - 3r}, \tag{93}$$

where $\mp$ corresponds to the upper and the lower family of the circular geodetics. $\pm$ corresponds to the two possible solutions of Eq. (92). The local extrema of the function $a_{\rm ms}(r,b)$ are given by the relation

$$a_{\rm ms(extr)} \equiv \mp (2\sqrt{b} \pm \sqrt{b(4b-1)}). \tag{94}$$

Thus, it can be shown that there is no solution for Eq. (92) related to the lower family of circular geodesics when

$$b > \frac{5}{4} \wedge a < -2\sqrt{b} + \sqrt{b(4b-1)}, \tag{95}$$

and there is no solution for the upper sign family of circular geodesics when $1 > b > 1/4$ and

$$2\sqrt{b} - \sqrt{b(4b-1)} < a < 2\sqrt{b} + \sqrt{b(4b-1)}. \tag{96}$$

The existence of the marginally stable circular geodesics dependent on the dimensionless parameters of the braneworld Kerr-Newman spacetimes is represented in Fig. 5. This figure will be crucial for construction of the classification of the Kerr-Newman spacetimes according to the Keplerian accretion, but it is not sufficient, as the classification of the photon circular geodesics plays a crucial role, too.

The function $a_{\rm ms}(r,b)$ determines, in a given Kerr-Newman spacetime, the location of the marginally stable circular geodesics that are usually considered to be the boundaries of the Keplerian accretion disks determined by the quasigeodesic motion.

B. Innermost stable circular geodesics

The standard treatment when the inner edge of the Keplerian accretion disks is located at the marginally stable orbits defined by the inflection point of the effective potential [this point is also the innermost stable circular orbit (ISCO) [55]] works perfectly in the braneworld Kerr-Newman black hole spacetimes, but the situation is more complex in the braneworld naked singularity spacetimes, as the ISCOs do not always correspond to the marginally

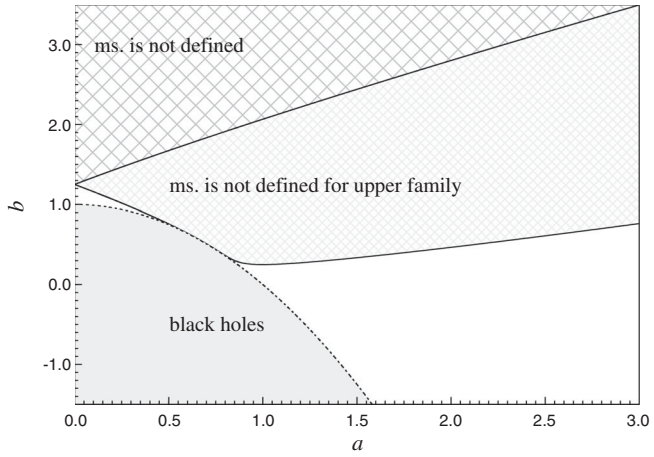

FIG. 5. Mapping of existence of the marginally stable circular geodesics in the parameter space of the braneworld Kerr-Newman spacetimes.

stable orbit defined by Eq. (92) [64]. The ISCOs that are not coinciding with a marginally stable circular geodesic, related to an inflection point of the effective potential, correspond to the orbits with the lowest radius in the sequence of stable circular geodesics. Contrary to the case of the marginally stable circular orbits from which the particles can move inwards, in the case of ISCOs representing the inner limit of stable circular geodesics, the particle remains captured at this orbit or in its vicinity. Such ISCO orbits were found for the first time in the Reissner-Nordstrom(–de Sitter) naked singularity spacetimes when they corresponded to orbits with vanishing angular momentum (particles at static positions) [15,16]. Here, we demonstrate the existence of a new class of this kind of ISCO representing the limit of stable circular geodesics located at the stable photon circular geodesic. In order to allow for the standard accretion with decreasing E's and L's with a decreasing radius of the stable orbits, we consider the stable circular geodesics with $E \to -\infty$ and $L \to -\infty$.

The ISCO can be formally determined if we consider the function of the radius of the circular geodesic $r_c(L_c; a, b)$, given implicitly by Eq. (56), or $r_c(E_c; a, b)$, given implicitly by Eq. (55). Then the $r_{\rm ISCO}$ can be defined in a given spacetime, with fixed parameters a, b, by the relations $dr_c/dL_c = 0$, $dr_c/dE_c = 0$, which can be expressed as $dL_c/dr_c \to -\infty$ and $dE_c/dr_c \to -\infty$, related to the standard accretion with decreasing energy and angular momentum of accreting matter. Note that the conditions $dL_c/dr_c \to \infty$ and $dE_c/dr_c \to \infty$ can determine the outermost stable circular geodesics from which the accretion could start, but such a situation is not related to a plausible astrophysical situation, as discussed in detail in [60].

There are two relevant cases where the conditions $dL_c/dr_c \to \pm\infty$ and $dE_c/dr_c \to \pm\infty$ can be satisfied:

$$\text{(a)} \quad 0 = r^2 - 3r + 2b \pm 2a\sqrt{r-b}, \tag{97}$$

$$\text{(b)} \quad r = b. \tag{98}$$

Case (a) tells us that the innermost circular geodesics correspond to the photon circular geodesics that can also be stable with respect to radial perturbations, so this condition is also applicable as a limit on the stable circular orbits of the test particles, as demonstrated in [15]. Then the specific energy and the specific angular momentum tend asymptotically to $E \to \pm\infty$ and $L \to \pm\infty$, but the impact parameter $\lambda = L/E$ remains finite. The condition $r > b$ could restrict the condition implied by the photon circular geodesics. Here, we consider the case where $dL_c/dr_c \to -\infty$ and $dE_c/dr_c \to -\infty$.

Case (b) can be relevant to the braneworld spacetimes with the positive braneworld parameter b, as demonstrated in [15], where the effective potential $V_{\rm Eff}(r, b, L)$ for the Reissner-Nordström naked singularity spacetimes clearly demonstrates that the inner edge of the Keplerian disk is located at $r = b$, having $L = 0$, while no marginally stable circular orbits corresponding to an inflection point of the effective potential exist. Note that, in some spacetimes, the sequence of the stable circular geodesics can start at the outermost stable circular geodesic with $dL_c/dr_c \to +\infty$ and $dE_c/dr_c \to +\infty$ corresponding to the stable circular geodesic.

C. Effective potential dependence on specific angular momentum and analytical proof that the Keplerian accretion with infinite efficiency can exist in approximation to geodesic motion

The Keplerian accretion works if a continuous sequence of local minima of the effective potential with decreasing values of angular momentum L exists. In terms of the effective potential (67), conditions for the existence of the Keplerian accretion disks can be expressed in the form

$$\frac{\partial V_{\rm Eff}(r,a,b,L)}{\partial r} = 0,$$
$$\frac{\partial^2 V_{\rm Eff}(r,a,b,L)}{\partial r^2} \leq 0,$$
$$\frac{\partial V_{\rm Eff}(r,a,b,L)}{\partial L} < 0. \tag{99}$$

Along with the possibility of stopping this procedure by the inflection point of the effective potential, there is another possible way to negate the validity of these conditions:

$$\frac{\partial V_{\rm Eff}(r,a,b,L)}{\partial L} = 0, \tag{100}$$

which will be satisfied at a turning point where

$$L = L_{\rm T} \equiv \frac{\pm a(2r-b)}{r\sqrt{r^2-2r+b}}. \tag{101}$$

At this turning point, the minimum of the effective potential, given by $\partial V_{\rm eff}(r,a,b,L_{\rm T})/\partial r = 0$, is located where

$$\frac{r-b}{r^2\sqrt{r^2-2r+b}} = 0 \Rightarrow r = b. \tag{102}$$

In such situations, the inner edge of the Keplerian accretion disk is located at $r = b$. Putting this result into the definition of the function $L_{\rm T}$, we find

$$L_{\rm T}(r=b) = \frac{\pm ab}{b\sqrt{b(b-1)}} \Rightarrow b > 1. \tag{103}$$

We see that the effect of the existence of the lowest possible value of angular momentum L associated with local minima of effective potential occurs only for values of

the tidal charge $b > 1$ when Eq. (102) is well defined at $r > b$.

The second possible way the conditions (99) are not well matched is related to the situation when the local minima of the effective potential turn into an inflection point at r defined by (92).

Therefore, the inflection point of the effective potential is not always defined, if the tidal parameter $b > 5/4$, for the lower family solution of Eq. (92). In this case the Keplerian accretion stops at the point $r = b$, where the minimum of the effective potential starts to increase in energy level with a decreasing L.

On the other hand, for the upper family solution of Eq. (92), the situation becomes extraordinary and much more interesting for the tidal charge in the interval $1 > b > 1/4$ and the appropriately tuned spin a; then the inflection point of the effective potential does not exist. For this reason, the Keplerian accretion starting at large values of the angular momentum of accreting matter cannot be stopped, and it continues with no limit to unlimitedly large negative values of the angular momentum and unlimitedly large negative values of the energy.

Therefore, in this case, unrestricted mining of the energy due to the Keplerian accretion could occur. Of course, this mining has to be stopped—at least when the energy of the accreting matter starts to be comparable to the mass parameter of the Kerr-Newman naked singularity and the approximation of the test particle motion of matter in the disk is no longer valid.

VI. CLASSIFICATION OF BRANEWORLD KERR-NEWMAN SPACETIMES ACCORDING TO RADIAL PROFILES OF CIRCULAR GEODESICS

In order to create classifications of the braneworld Kerr-Newman black hole and naked singularity spacetimes according to possible regimes of the Keplerian accretion, we consider the existence of event horizons and the existence of the ergosphere, and we use the characteristics of the circular geodesics: existence of the circular photon geodesics and their stability, existence of the marginally stable circular geodesics related to inflection points of the effective potential, and relevance of the limiting radius $r = b$. We use the classification of the braneworld Kerr-Newman spacetimes introduced for the characterization of the photon circular geodesics, and we generate a subdivision of the introduced classes according to the criteria related to the marginally stable orbits.

The individual classes of the Kerr-Newman spacetimes will be represented by typical radial profiles of the specific angular momentum L, specific energy E, and effective potential V_{Eff} that enable understanding of the Keplerian accretion and calculation of its efficiency. We first briefly summarize the results of two special cases—Kerr and Reissner-Nordström spacetimes. In the following classification of the braneworld Kerr-Newman spacetimes, the characteristic types of behavior of the circular geodesics in the special Kerr and Reissner-Nordström spacetimes occur, but some quite new and extraordinary situations also arise. The results of the circular geodesic analysis in the braneworld Kerr-Newman spacetimes can also be directly applied to the circular geodesics in the standard Kerr-Newman spacetimes if we make the transformation $b \to Q^2$, where Q^2 represents the squared electric charge parameter of the Kerr-Newman background.

A. Case $b = 0$: Kerr black hole and naked singularity spacetimes

The limiting case of the well-known results of the test particle circular orbits in the Kerr spacetimes that were studied in detail in [35,43] demonstrates clearly the necessity of very carefully treating the families of circular orbits in the naked singularity spacetimes, where the simple decomposition of the circular orbits to corotating and counterrotating (retrograde) is not always possible. Namely, in the spacetimes with $1 < a < a_c = 1.3$, the circular orbits that are corotating at large distances from the ring singularity become retrograde near the ring singularity, at the ergosphere; moreover, in the spacetimes with $1 < a < a_0 = 1.089$, the covariant energy of such orbits can be negative. The specific energy and the specific angular momentum of the circular geodesics of the Kerr black hole and naked singularity spacetimes are illustrated in Fig. 8. Notice that the unstable circular geodesics approach the radius $r = 0$ with unlimitedly increasing covariant energy and axial angular momentum; however, the photon circular geodesic cannot exist at the ring singularity. The Kerr naked singularities are classically unstable, as the Keplerian accretion from both the corotating and counterrotating disks inverts the naked singularity into an extreme Kerr black hole—the transition is discontinuous (continuous) for corotating (counterrotating) Keplerian disks [34–36,65]. We shall see later that the Keplerian accretion cannot be generally treated simply in the Kerr-Newman naked singularity spacetimes due to the complexities that are discussed in detail in [60]. We expect to address this issue in future work.

B. Case $a = 0$: Reissner-Nordström black hole and naked singularity spacetimes

The other limiting case of the Reissner-Nordström (RN) and Reissner-Nordtröm–(anti–)de Sitter black hole and naked singularity spacetimes was treated in [15,16]. It has been demonstrated that in the Reissner-Nordström naked singularity spacetimes that even two separated regions of circular geodesics could exist. The doubled regions of stable circular motion could occur in the RN naked singularity spacetimes with the charge parameter $1 < Q^2 < 5/4$—or, even, only stable circular geodesics

could exist—if the charge parameter $Q^2 > 5/4$. In the RN naked singularity spacetimes doubled photon circular geodesics can also occur, with the inner one being stable relative to radial perturbations, if the charge parameter is in the interval $1 < Q^2 < 9/8$ [15,17]. The same phenomena occur in the naked singularity Kehagias-Sfetsos spacetimes of the Hořava quantum gravity [60,66] or in the no-horizon regular Bardeen or Ayon-Beato-Garcia spacetimes [67,68].

We shall see that, in the braneworld Kerr-Newman naked singularity spacetimes, the special naked singularity effects of the Kerr and Reissner-Nordström case are mixed in an extraordinary way, leading to the existence of an infinitely deep gravitational well and implying the new effect we call mining instability.

C. Characteristic points of the Kerr-Newman spacetime classification

The classification of the braneworld Kerr-Newman spacetimes according to the character of the circular geodesics and the related effective potential are determined by the functions governing the local extrema of the functions giving the photon circular geodesics and the marginally stable circular geodesics corresponding to the inflection points of the effective potential. In the space of the spacetime parameters b-a, 14 regions then exist corresponding to classes of the braneworld Kerr-Newman spacetimes, demonstrating the different behaviors of the circular geodesics and the Keplerian accretion, as demonstrated in Figs. 6 and 7, giving details of the regions of low values of the dimensionless parameters a and b. These regions are governed by intersection points of the curves (88) and (94), which give 13 characteristic points in the parameter space that are summarized in the following way: the pairs (a, b) are ordered gradually from top to the bottom and from left to the right,

$$
\begin{aligned}
&(1) \to (0, 1.25),\\
&(2) \to (0, 1.125),\\
&(3) \to \left(\frac{A_-(12+A_-)}{16\sqrt{2}}, \frac{3}{32}(12+A_-)\right)\\
&\quad = (0.0831, 1.1748),\\
&(4) \to \left(\frac{1}{3\sqrt{3}}, 1\right) = (0.19245, 1),\\
&(5) \to (2-\sqrt{3}, 1) = (0.268, 1),\\
&(6) \to \left(0.5, \frac{3}{4}\right),\\
&(7) \to (\sqrt{0.5}, 0.5),\\
&(8) \to (1, 0.25),\\
&(9) \to (2+\sqrt{3}, 1) = (3.732, 1),\\
&(10) \to \left(\frac{A_+(12+A_+)}{16\sqrt{2}}, \frac{3}{32}(12+A_+)\right)\\
&\quad = (15.0992, 5.361),
\end{aligned}
$$

where

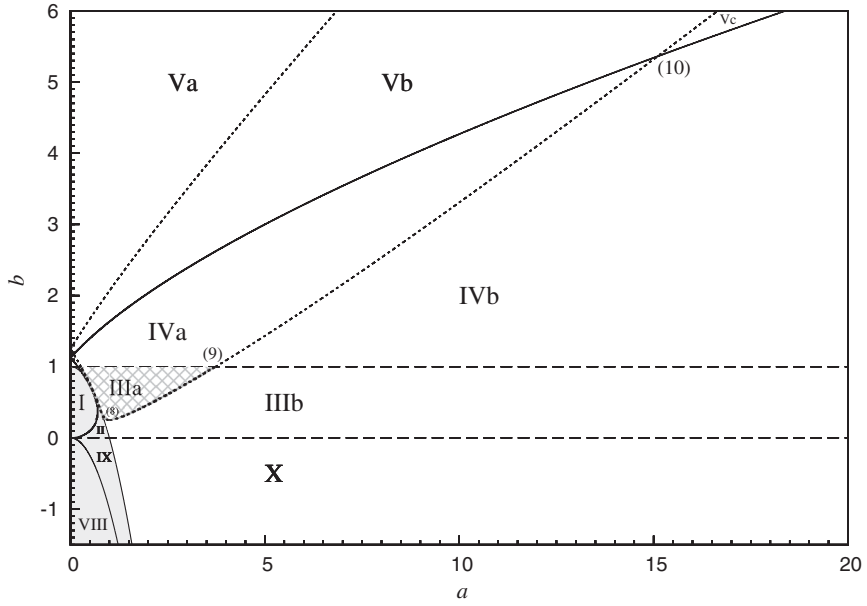

FIG. 6. Classification of the braneworld Kerr-Newman spacetimes according to the properties of circular geodesics relevant to the Keplerian accretion. The parameter space b-a is separated by curves governing the extrema of the functions determining the photon circular orbits (the solid lines) and the marginally stable orbits (the dashed lines). Point $(\sqrt{0.5}, 0.5)$ is an intersection of the dashed line and the curve separating black holes from naked singularities ($b = 1 - a^2$). These two curves are tangent at the common point.

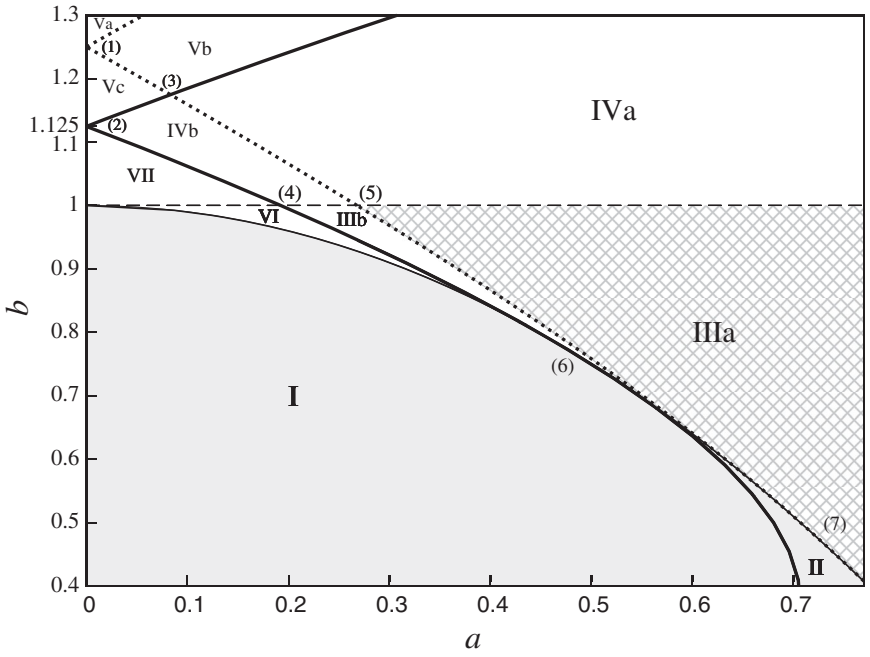

FIG. 7. Classification of the braneworld Kerr-Newman spacetimes according to the properties of circular geodesics relevant to the Keplerian accretion. The parameter space b-a is separated by curves governing the extrema of the functions determining the photon circular orbits (the solid lines) and the marginally stable orbits (the dashed lines). Detailed structure for small values of spin a and $b \sim 1$.

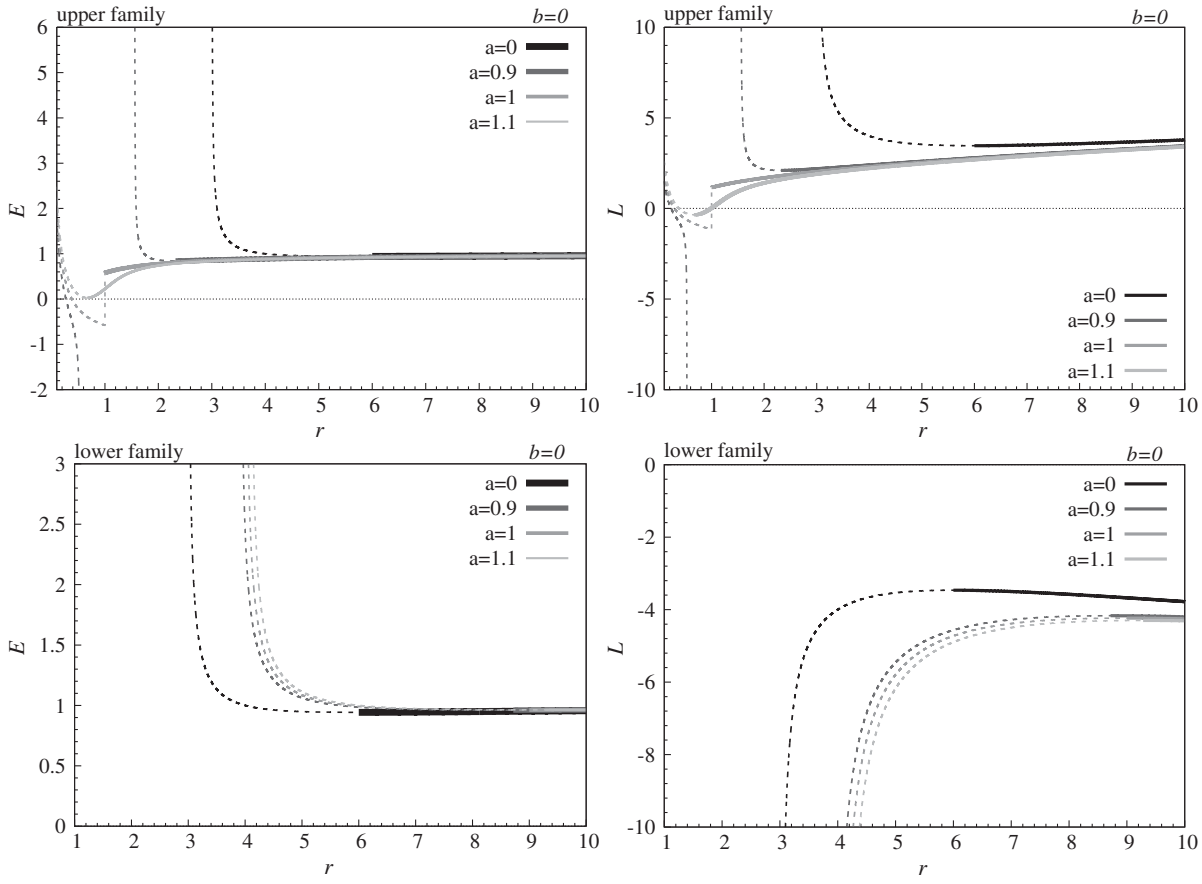

FIG. 8. E and L for Kerr black holes and naked singularities.

$$A_{\pm} = (9 + 8\sqrt{3} \pm \sqrt{3(83 + 48\sqrt{3})}). \quad (104)$$

Point (6) is the crossing point of the function of the extrema of the photon circular orbit function $a_{\text{ph-ex}}$, and the curve separating the black hole and naked singularity spacetimes, $b = 1 - a^2$. Point (7) is the common point of the dotted curve, given by the function $a_{\text{ms(extr)}}$ and limiting the spacetimes, allowing for the existence of marginally stable orbits, and the curve separating the black holes from naked singularities ($b = 1 - a^2$). These two curves are tangent at the common point.

D. Character of circular geodesics in the Kerr-Newman spacetimes

The parameter space of the braneworld Kerr-Newman spacetimes b-a is divided into 14 regions due to the criteria reflecting basic properties of the spacetimes and properties of their circular geodesics:

(i) Existence of event horizons and an ergosphere.
(ii) Existence of unstable and stable circular photon geodesics.
(iii) Existence of the marginally stable geodesics or the ISCO.

The classification is summarized in Table III. Basically, we combine Figs. 5 and 4 to obtain Figs. 6 and 7, where properties of the photon circular geodesics and properties of the marginally stable geodesics or ISCOs are reflected. We will show that the most surprising properties of the Keplerian accretion arise in the spacetimes of class IIIa.

TABLE III. Classification of parameter space b-a with respect to ISCO—radius of the innermost stable circular orbit; MSO(u)—radius of the marginally stable orbit for the upper sign family; MSO(l)—radius of the marginally stable orbit for the lower sign family; SP—number of stable photon circular orbits; UP—number of unstable photon circular orbits. ISCO has only two possible outcomes. It can either be identical to the MSO or lie at $r = b$. The word "classic" in this context means that MSO is defined by Eq. (92).

Class	ISCO	MSO(u)	MSO(l)	Hor./Erg.	SP	UP
I	= MSO	classic	classic	yes/yes	0	2
II	= MSO	classic	classic	yes/yes	1	3
IIIa	= Photon	⋯	classic	no/yes	1	1
IIIb	= MSO	classic	classic	no/yes	1	1
IVa	at $r = b$	⋯	classic	no/no	1	1
IVb	at $r = b$	classic	classic	no/no	1	1
Va	at $r = b$	⋯	⋯	no/no	0	0
Vb	at $r = b$	⋯	classic	no/no	0	0
Vc	at $r = b$	classic	classic	no/no	0	0
VI	= MSO	classic	classic	no/yes	2	2
VII	at $r = b$	classic	classic	no/no	2	2
VIII	= MSO	classic	classic	yes/yes	0	2
IX	= MSO	classic	classic	yes/yes	0	3
X	= MSO	classic	classic	no/yes	0	1

Now we give properties of the circular geodesics in all 14 classes of the braneworld Kerr-Newman spacetimes, presenting and discussing the typical radial profiles of their specific energy and specific angular momentum, complemented by sequences of the effective potential. Classification of the standard Kerr-Newman spacetimes according to properties of the circular geodesics contains all of the classes except those related to $b < 0$; therefore, classes VIII, IX, and X are excluded.

1. Class I

This class (Fig. 9) of black hole spacetimes has two horizons, two unstable photon circular orbits, and an ergosphere. The class border is given by the line $b = a_{\text{ph-ex}}(r = 4b/3, b)$, $b = 1 - a^2$, with the intersection at point $(0.5, 3/4)$ [point (6) in Fig. 6] and line $a = 0$.

Marginally stable orbits for test massive particles are given by the inflection point of the effective potential are defined by Eq. (92) and coincide with the ISCOs (this is the standard scenario of the Keplerian accretion: for short, classic).

2. Class II

This class (Fig. 10) of black hole spacetimes has two horizons, one stable and three unstable photon circular orbits, and an ergosphere. Notice that the stable and unstable photon circular geodesics are located under the inner horizon and thus are irrelevant for the Keplerian accretion. The border is given by the line $b = a_{\text{ph-ex}}(r = 4b/3, b)$ and $b = 1 - a^2$, with the intersection being at point $(0.5, 3/4)$ [point (6) in Fig. 6] and line $b = 0$.

Marginally stable orbits for test massive particles are given by the inflection point of the effective potential, coinciding with the ISCOs (classic).

3. Class IIIa

This class (Fig. 11) of naked singularity spacetimes has one stable and one unstable photon circular geodesic and an ergosphere. The border of the class IIIa region is given by the lines $b = a_{\text{ms(extr)}}$ and $b = 1$, with intersection points at $(2 - \sqrt{3}, 1) = (0.268, 1)$ [point (5)] and $(2 + \sqrt{3}, 1) = (3.732, 1)$ [point (9)]. We have also marked point (7) with coordinates $(\sqrt{0.5}, 0.5)$, where the lines $b = a_{\text{ms(extr)}}$ and $b = 1 - a^2$ touch and are tangent to each other. This theoretically means that an effect of mining instability can be achieved for extremal Kerr-Newman black holes with spin parameter $a = \sqrt{0.5}$ and the charge or braneworld tidal charge parameter $b = 0.5$. However, it occurs under the event horizon. We have also marked point (8) with coordinates (1, 0.25), giving information on the minimal amount of the electric charge or braneworld tidal charge parameter b.

The marginally stable orbit of the massive test particles is in the case of the lower family circular geodesics given by the inflection point of the effective potential, and it coincides with the ISCO (classic).

In the case of the upper family circular geodesics, the inflection point of the effective potential is not defined and the sequence of minima of the effective potential continues with decreasing specific energy and specific angular momentum of the accreting matter down to the stable photon orbit. This orbit can therefore be considered an ISCO of the massive test particles. We have thus found an infinitely deep gravitational well enabling, theoretically, an unlimited mining of energy from the naked singularity. In fact, such a mining instability could work only up to the energy contained in the naked singularity spacetime. We can expect that the energy mining could also work in more realistic situations where the naked singularity is removed and an astrophysically more plausible superspinar is created by joining a regular (e.g., stringy) solution to the Kerr-Newman spacetime at a radius overcoming the outer radius of the causality violation region [37,40]. The mining could work if the matching radius of the internal stringy spacetime and the outer Kerr-Newman spacetime is smaller than the radius of the stable photon orbit related to the mining instability of the class IIIa spacetimes.

For completeness, we also give in this case the locally measured (LNRF) specific energy of the upper family circular geodesics. As shown in Fig. 12, the specific energy E_{LNRF} diverges, along with the covariant specific energy E as the orbit approaches the limiting photon circular orbit. On the other hand, Fig. 13 clearly demonstrates that the ratio $|E|/E_{\mathrm{LNRF}}$ remains finite while the orbits approach the location corresponding to the stable photon circular orbit.

Of course, the mining instability could work only if the assumption of the test particle motion of the accreting matter is satisfied. Therefore, the assumption requires validity of the relation

$$|\tilde{E}| \ll M, \tag{105}$$

and the covariant energy of the particle (accreting matter) has to be much smaller than the naked singularity mass parameter M. Of course, the issue of the mining instability and the related interaction of the mining-unstable Kerr-Newman naked singularity (the Kerr-Newman superspinar) and the accreting mass is much more complex and deserves a more detailed study.

4. Class IIIb

This class (Fig. 14) of naked singularity spacetimes has one stable and one unstable photon circular orbit and an ergosphere. In the parameter space b-a, the area related to this class is not compact and disintegrates into two separated areas. The first area is infinitely large: its border is given by lines $b = a_{\mathrm{ms(extr)}}$, $b = 1 - a^2$, $b = 1$, and $b = 0$, with intersections at the point $(\sqrt{0.5}, 0.5)$ [point (7)] and $(2 + \sqrt{3}, 1)$ [point (9)]. The second area is compact and finite. Its border is given by lines $b = a_{\mathrm{ms(extr)}}$, $b = a_{\mathrm{ph\text{-}ex}}(r = 4b/3, b)$, $b = 1 - a^2$, and $b = 1$, with intersection points (4), (5), and (7). It is not obvious from the figures, but $b = a_{\mathrm{ms(extr)}}$ and $b = a_{\mathrm{ph\text{-}ex}}(r = 4b/3, b)$ do not intersect.

Marginally stable orbits of both the lower and the upper family of circular geodesics are given by the inflection point of the effective potential and coincide with the ISCOs (classic). Notice that in this case the sequence of the upper family orbits with descending specific energy E and specific angular momentum L is interrupted by a sequence where both E and L increase with a decreasing radius, thus corresponding to the unstable geodesics. In this case, the infinitely deep gravitational well still exists, but the Keplerian accretion sequence is interrupted and this gravitational well cannot be applied in an astrophysically natural accretion process. Nevertheless, it is still possible to use this gravitational well, if matter with appropriate initial conditions (values of the motion constants), enabling the start of the mining instability, could appear close to the naked singularity.

5. Class IVa

This class (Fig. 15) of naked singularity spacetimes has one stable and one unstable photon circular orbit. The class is without an ergosphere. The border of this class in the spacetime parameter space is given by the lines

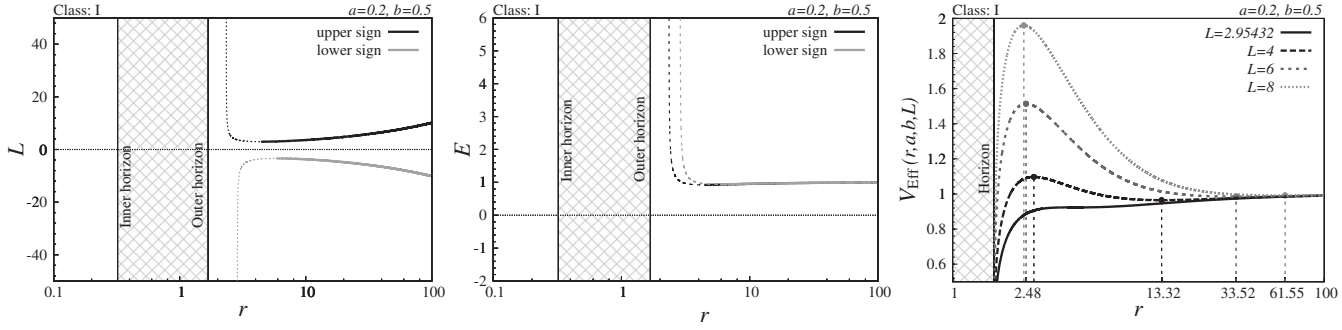

FIG. 9. L, E, and effective potential for class I.

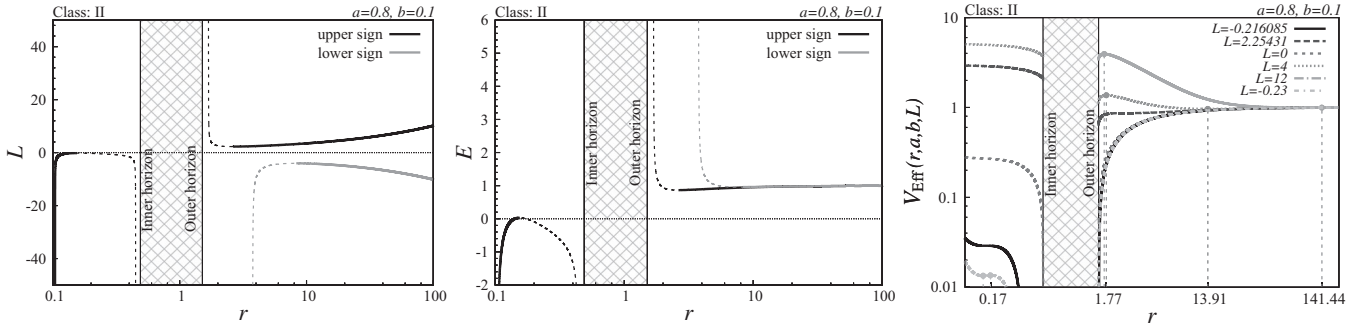

FIG. 10. L, E, and effective potential for class II.

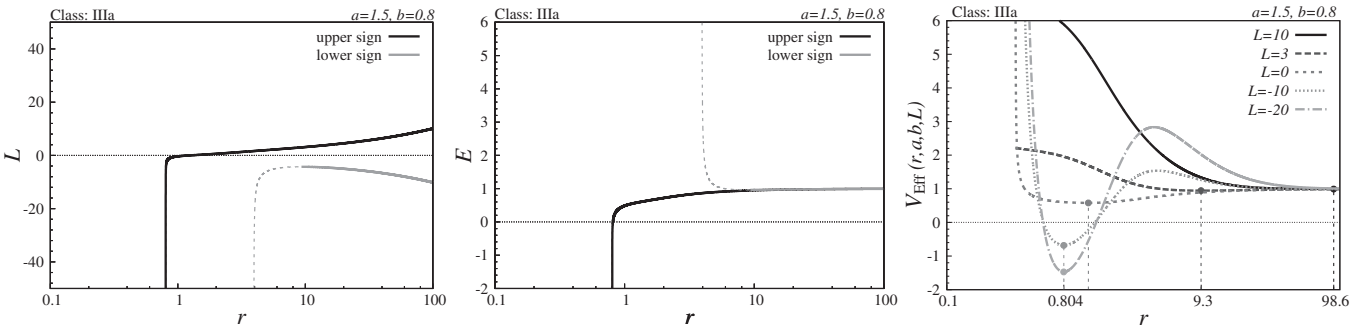

FIG. 11. L, E, and effective potential for class IIIa.

$b = a_{\text{ph-ex}}(r = 4b/3, b)$ and $b = a_{\text{ms(extr)}}$, with intersection points (3), (5), (9), and (10).

For the lower family circular geodesics, the marginally stable orbits defined by the inflection point of the effective potential occur (classic). For the upper family, the circular geodesics' marginally stable orbit is not defined, and the ISCO is located at $r = b$, as it is for all classes with $b > 1$. A sequence of stable circular geodesics with sharply increasing specific energy occurs near (slightly above) the radius $r = b$, approaching the stable photon circular orbit. (Such sequences of stable circular orbits are discussed in [60].)

Note that the probability that we are actually living in a spacetime with the braneworld tidal charge parameter greater than one is very small [26,27].

6. Class IVb

This class (Fig. 16) of naked singularity spacetimes has one stable and one unstable photon circular orbit. These spacetimes are without an ergosphere. In the parameter space b-a, this class is not compact and disintegrates into two separated areas. The first area is infinitely large: the border is given by the lines $b = a_{\text{ph}}(4b/3, b)$, $b = a_{\text{ms(extr)}}$,

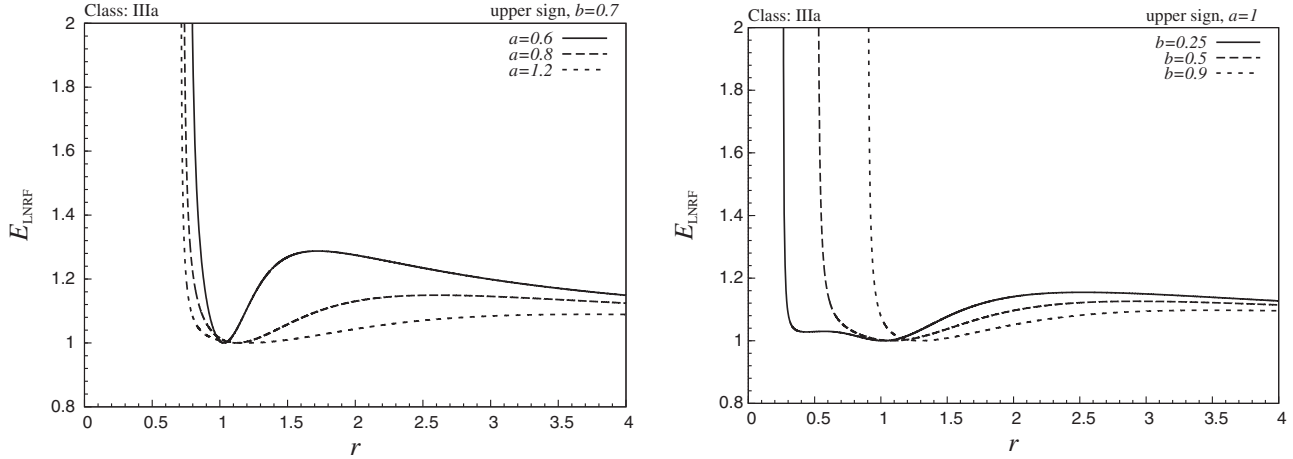

FIG. 12. Energy measured by the LNRF observers (upper sign family orbits only) in the mining-unstable Kerr-Newman spacetimes of class IIIa. The energy diverges at the radius of the stable photon circular orbit.

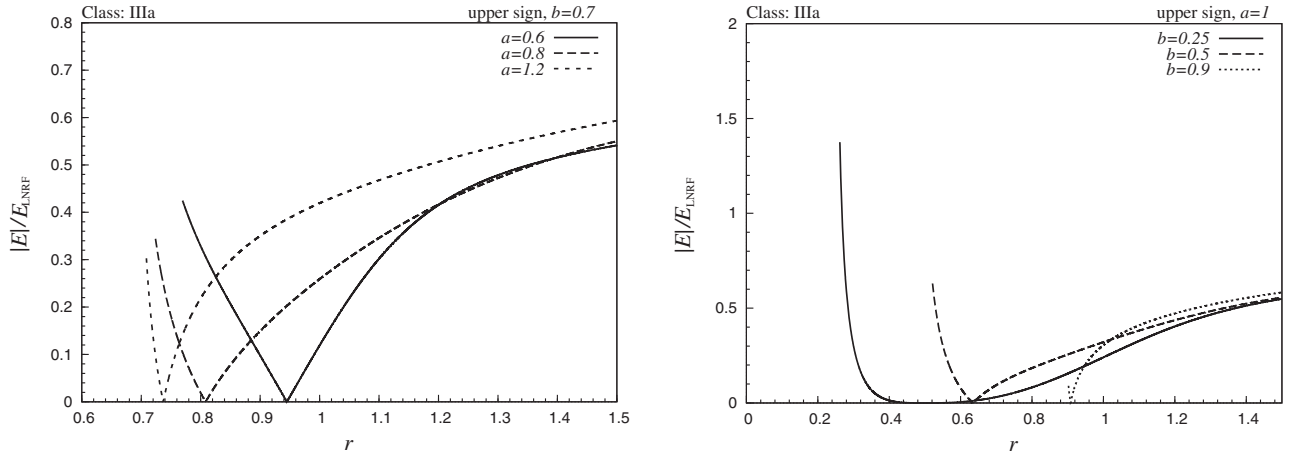

FIG. 13. Absolute value of covariant energy $|E|$ divided by LNRF energy (for the upper sign family orbits) in the mining-unstable Kerr-Newman spacetimes of class IIIa. The fraction is defined down to the radius of the stable circular photon orbit, and at this point it has a finite value.

and $b = 1$, with intersection points (9) and (10). The second area is finite and its border is given by the same lines and intersection points (2), (3), (4), and (5).

For both the upper and lower families of the circular geodesics, the marginally stable orbits of the test massive particles are given by the inflection point of the effective potential, governing the sequence of geodesics related to the standard Keplerian accretion (classic). There is an additional internal sequence for a stable circular geodesic, with the ISCO located at $r = b$, as it is for all classes with $b > 1$. This sequence approaches the stable photon circular geodesic at the outer edge.

7. Class Va

This class (Fig. 17) of naked singularity spacetimes has no stable or unstable photon circular orbits. These spacetimes are also without an ergosphere. The border of the class Va region in the parameter space is given by the lines $b = a_{\mathrm{ms(extr)}}$ and $a = 0$, with intersection point (1).

For both the lower and upper family circular geodesics, the marginally stable orbits are not defined. The circular geodesics are only stable and the ISCOs are located at $r = b$, as they are for all spacetime classes with $b > 1$.

8. Class Vb

This class (Fig. 18) of naked singularity spacetimes has no stable or unstable photon circular orbits. These spacetimes are also without an ergosphere. The border of the class Vb region in the parameter space is given by the lines $b = a_{\mathrm{ms(extr)}}$ and $b = a_{\mathrm{ph}}(4b/3, b)$, with intersection points (1), (3), and (10). The class is infinitely extended in the parameter space.

The upper family circular geodesics are stable only, finishing at the ISCO located at $r = b$. The marginally stable orbit exists for the lower family orbits, giving the limit of the standard Keplerian accretion. The lower family orbits continue downwards by a sequence of unstable orbits and, finally, stable orbits finishing at $r = b$.

9. Class Vc

This class (Fig. 19) of naked singularity spacetimes has no stable or unstable photon circular orbits. These are again spacetimes without an ergosphere. In the parameter space b-a, this class disintegrates into two separated areas. The first one is infinitely extended: its border is given by the lines $b = a_{\mathrm{ph\text{-}ex}}(r = 4b/3, b)$ and $b = a_{\mathrm{ms(extr)}}$, with

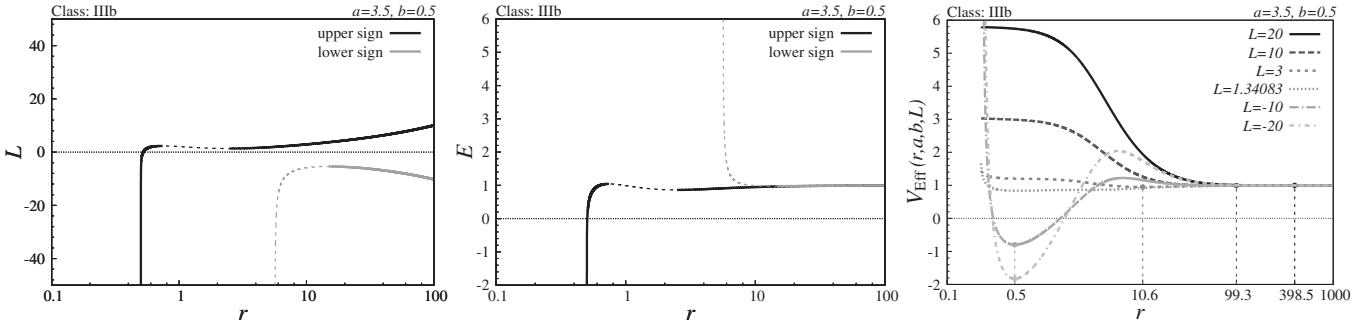

FIG. 14. L, E, and effective potential for class IIIb.

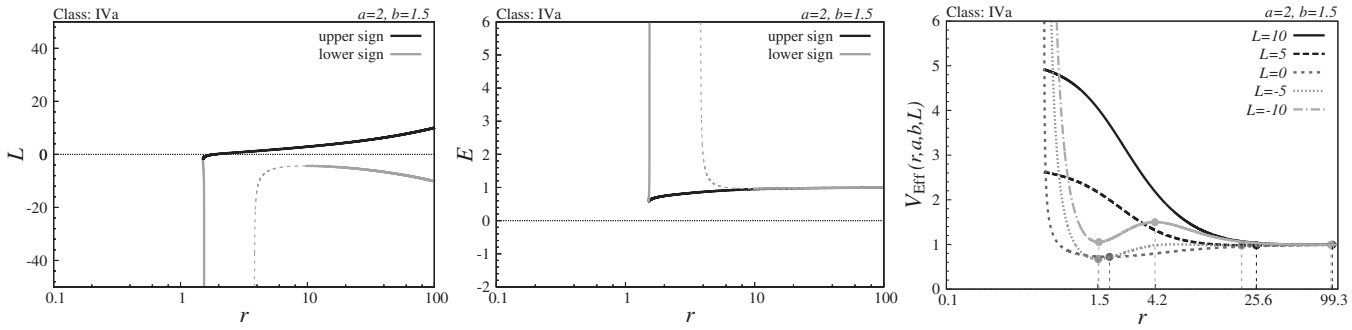

FIG. 15. L, E, and effective potential for class IVa.

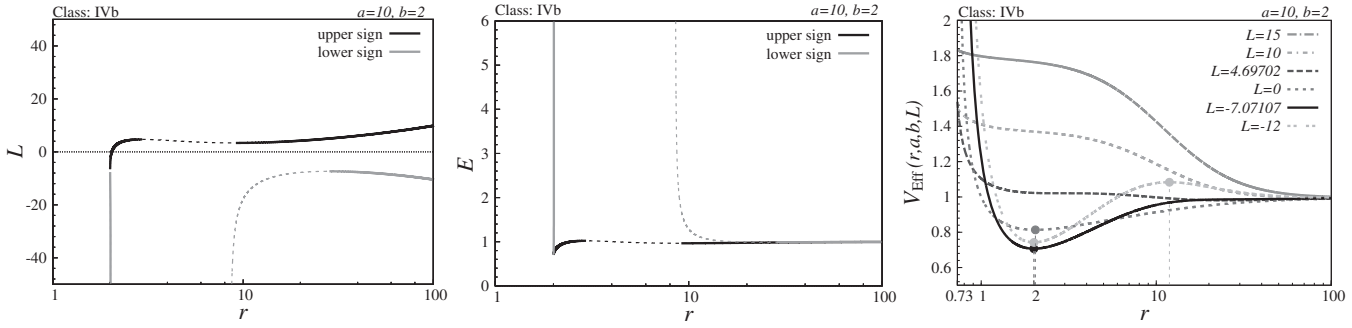

FIG. 16. L, E, and effective potential for class IVb.

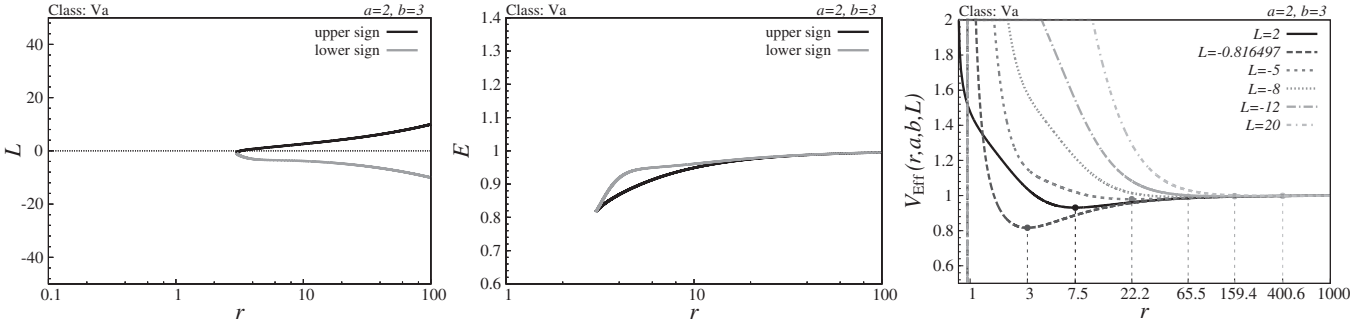

FIG. 17. L, E, and effective potential for class Va.

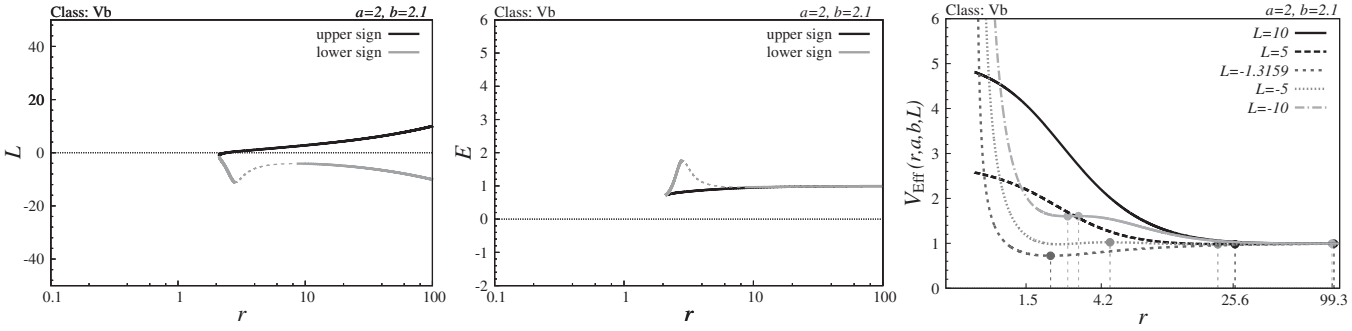

FIG. 18. L, E, and effective potential for class Vb.

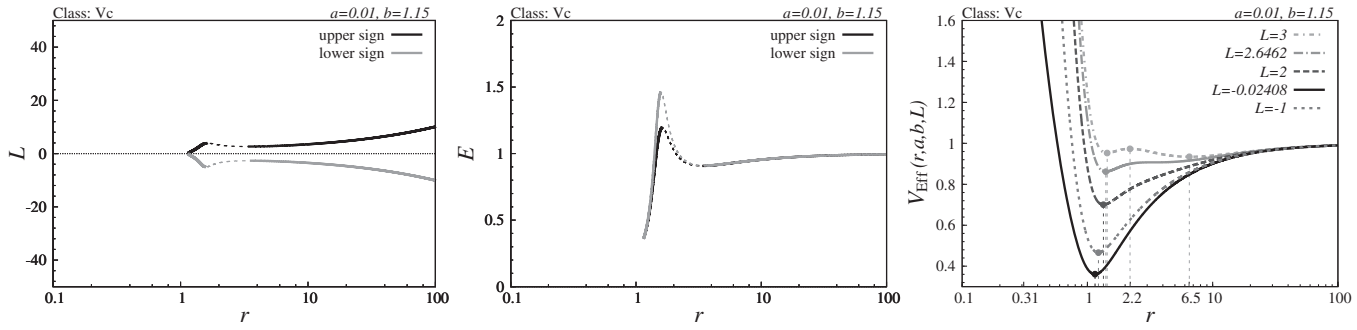

FIG. 19. L, E, and effective potential for class Vc.

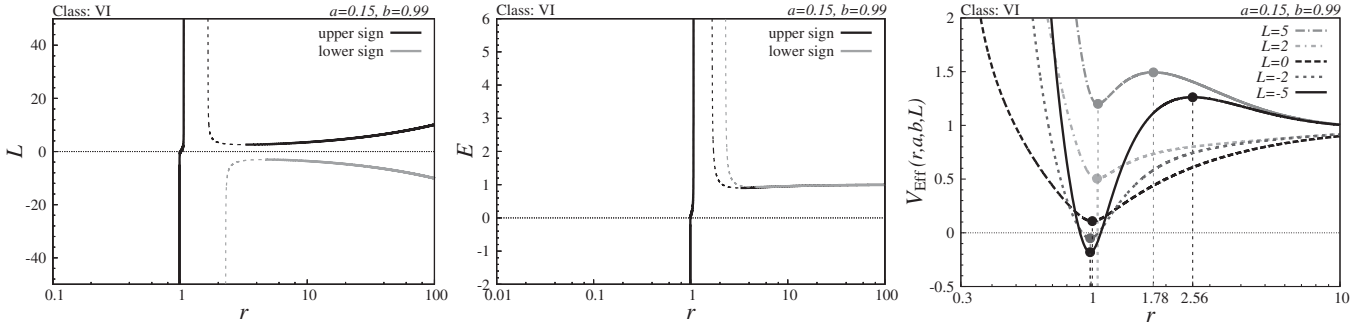

FIG. 20. L, E, and effective potential for class VI.

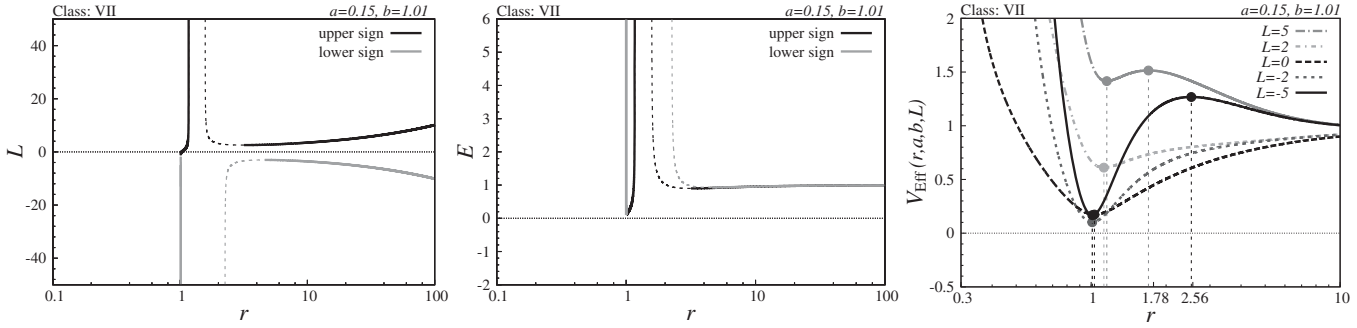

FIG. 21. L, E, and effective potential for class VII.

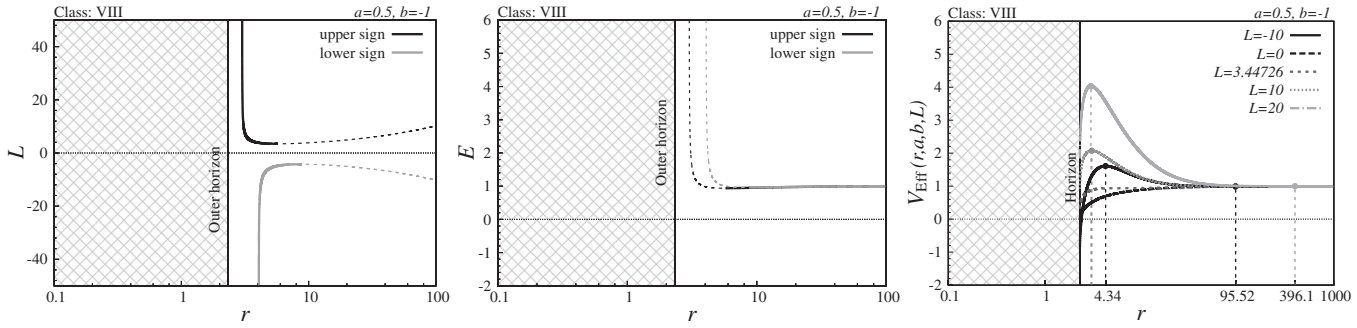

FIG. 22. L, E, and effective potential for class VIII.

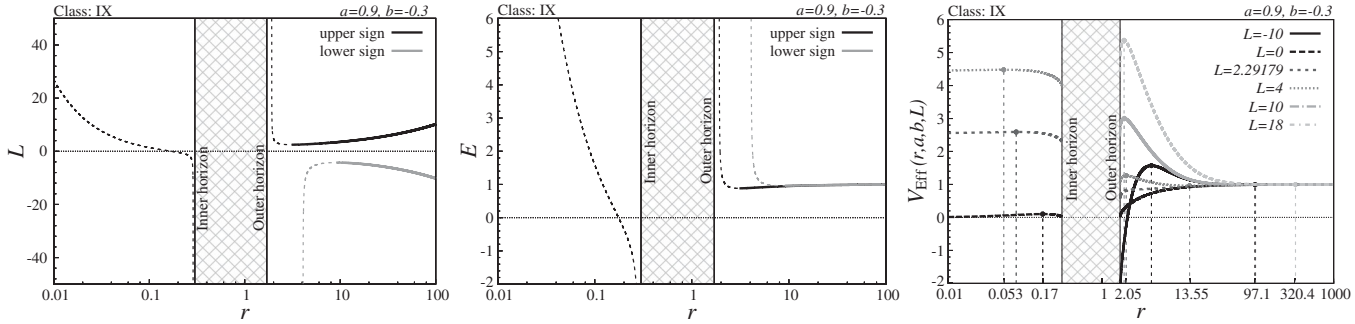

FIG. 23. L, E, and effective potential for class IX.

intersection point (10). The second area is finite and its border is given by lines $b = a_{\mathrm{ph\text{-}ex}}(r = 4b/3, b)$, $b = a_{\mathrm{ms(extr)}}$, and $a = 0$, with intersection points (1), (2), and (3).

The marginally stable orbit exists for both the lower and upper family circular geodesics, thus giving the standard limit of the Keplerian accretion (classic). Both the lower and upper family orbits continue downwards by a sequence of unstable orbits and, finally, stable orbits finishing at $r = b$.

10. Class VI

This class (Fig. 20) of naked singularity spacetimes has two stable and two unstable photon circular orbits and an ergosphere. In the parameter space, the area of the class VI spacetimes has the boundary given by the lines $b = a_{\mathrm{ph\text{-}ex}}(r = 4b/3, b)$, $b = 1 - a^2$, and $b = 1$, with intersection points (4) and (6).

For both the lower and the upper family of circular geodesics, the marginally stable orbit exists, thus giving the inner edge of the standard Keplerian accretion. The upper family orbits have also a very narrow region of stable circular orbits near the radius $r = b$, starting with the stable circular photon orbit.

11. Class VII

This class (Fig. 21) of naked singularity spacetimes has two stable and two unstable photon circular orbits, with no ergosphere. In the parameter space, the area of the class VII spacetimes has the boundary given by the lines $b = a_{\mathrm{ph\text{-}ex}}(r = 4b/3, b)$, $a = 0$, and $b = 1$, with intersection points (2) and (4).

For both the lower and upper family circular geodesics, the marginally stable orbit exists, thus giving the edge of the standard Keplerian accretion. Furthermore, both the lower and upper family orbits have the ISCO at $r = b$, where the sequence of stable orbits finishes, starting for each family at the related photon circular geodesic.

12. Class VIII

This class (Fig. 22) of black hole spacetimes has a negative braneworld tidal charge parameter b—which has only one horizon, located at $r > 0$—two unstable photon circular orbits, and an ergosphere. In the parameter space b-a, the boundary of the region related to this class is given by the lines $b = -a^2$ and $a = 0$.

For both the lower and upper family circular geodesics, the marginally stable orbit exists, determining the inner edge of the standard Keplerian disk. Thus, we obtained the standard situation typical for Kerr black holes, but no geodesic structure occurs at $r > 0$ under the event horizon.

13. Class IX

This class (Fig. 23) of black hole spacetimes has a negative braneworld parameter b with two horizons, three unstable photon circular orbits, and an ergosphere. The border of the related region of the spacetime parameter space is given by the lines $b = 1 - a^2$, $b = -a^2$, and $b = 0$.

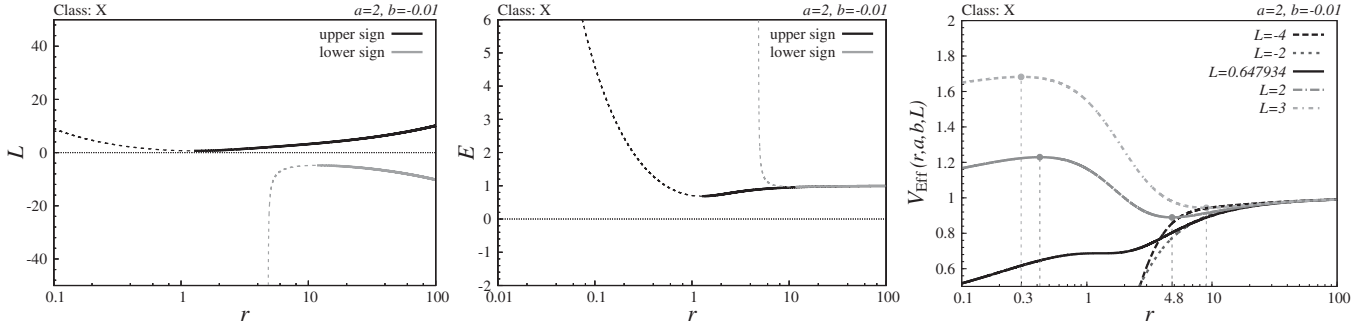

FIG. 24. L, E, and effective potential for class X.

For both the lower and upper circular orbits, the marginally stable orbit exists, giving in a standard way the inner edge of the Keplerian accretion. Unstable orbits exist under the inner horizon.

14. Class X

This class (Fig. 24) of naked singularity spacetimes has a negative brane parameter b with one unstable photon circular orbit and an ergosphere. The border of the related region of the parameter space is given by the lines $b = 1 - a^2$ and $b = 0$.

In these naked singularity spacetimes, the marginally stable orbit exists for both the lower and the upper family of circular geodesics, thus representing in both cases the inner edge of the Keplerian accretion disks. Under the marginally stable orbits, only unstable orbits exist for both families. From the point of view of the geodesic structure, the naked singularity spacetimes of class X resemble the standard Kerr naked singularity spacetimes.

VII. EFFICIENCY OF THE KEPLERIAN ACCRETION

Now we are able to determine the energetic efficiency of the Keplerian accretion. From the astrophysical point of view, the standard Keplerian accretion is relevant in the regions enabling the start of accretion at large distance (infinity) and its completion at the first inner edge that can be approached by a continuous accretion process. We determine the efficiency of the Keplerian accretion for all classes of the braneworld Kerr-Newman spacetimes for the standard Keplerian accretion. In some of these spacetimes, an inner region also exists where the Keplerian accretion could work due to the decline of both energy and angular momentum with a decreasing radius. However, these regions are not related to the standard notion of Keplerian accretion and will not be considered here for calculations of the accretion efficiency. Moreover, complexities of the Keplerian accretion process related to the behavior of the angular velocity could also exist. These complexities are described in detail in [60]—we shall not discuss these subtleties in this paper.

We concentrate our attention on determining the efficiency for the Keplerian accretion following the upper family circular geodesics, where the efficiency can be very high, being in some cases even unlimitedly high (formally). In the case of the upper family Keplerian accretion, the efficiency is discontinuous when the transition between the naked singularity with sufficiently high dimensionless spin and the related extreme black hole state is considered. The critical values of the spin and the related critical tidal charge read

$$a_{\rm cr} = \frac{1}{\sqrt{2}}, \qquad b_{\rm cr} = \frac{1}{2}. \tag{106}$$

We must stress that the efficiency of the Keplerian accretion in the near-extreme naked singularity spacetimes exceeds significantly the efficiency in the extreme black hole spacetimes. On the other hand, the efficiency of the Keplerian accretion in the upper family regime is fully continuous in the case of the transition of the naked singularity to an extreme black hole spacetime with sufficiently low spin, $a < a_{\rm cr}$, and for all the braneworld Kerr-Newman (KN) spacetimes in the case of the Keplerian accretion in the lower family accretion regime. Generally, the efficiency of the Keplerian accretion is substantially smaller in comparison to the upper family regime in a given Kerr-Newman spacetime.

The efficiency of the accretion for the geometrically thin Keplerian disks governed by the circular geodesics is defined by the relation

$$\eta(a, b) = 1 - E(r_{\rm edge}, a, b), \tag{107}$$

where $r_{\rm edge}$ denotes the location of the inner edge of the standard Keplerian accretion disks. For the Keplerian disks following the lower family circular geodesics, the inner edge of the disk is always located at the marginally stable geodesic, thus giving always the scenario of the Keplerian accretion in the Kerr spacetimes. On the other hand, for the upper family Keplerian disks, the situation is more complex, as follows from the classification of the braneworld Kerr-Newman spacetimes. Three qualitatively different cases can occur that depend on combinations of the dimensionless spacetime parameters a and b.

In the first family of classes of the Kerr-Newman spacetimes, the $r_{\rm edge}$ is simply located at the marginally stable geodesic, thus giving the scenario of the Keplerian accretion onto Kerr black holes—this case includes all of the braneworld Kerr-Newman black hole spacetimes.

In the second family of the Kerr-Newman classes, the inner edge of the Keplerian disk is located at the radius $r = b$, thus giving the special case first discovered for the Reissner-Nordström naked singularity spacetimes [15,16]. In all classes with $b > 1$ (IV, V), the efficiency of the Keplerian accretion along the upper family of circular geodesics is independent of the spin parameter a being defined by the simple relation [69]

$$\eta(b) = 1 - \sqrt{1 - \frac{1}{b}}. \tag{108}$$

The efficiency goes slowly to 0% for $b \to \infty$; see Fig. 25.

In the third and most interesting family of the Kerr-Newman spacetime classes, $r_{\rm edge}$ corresponds to the radius of the stable photon orbit approached by particles with the specific energy $E \to -\infty$ and the specific angular momentum $L \to -\infty$. Notice that the limiting photon circular geodesic is a corotating one, as the impact parameter

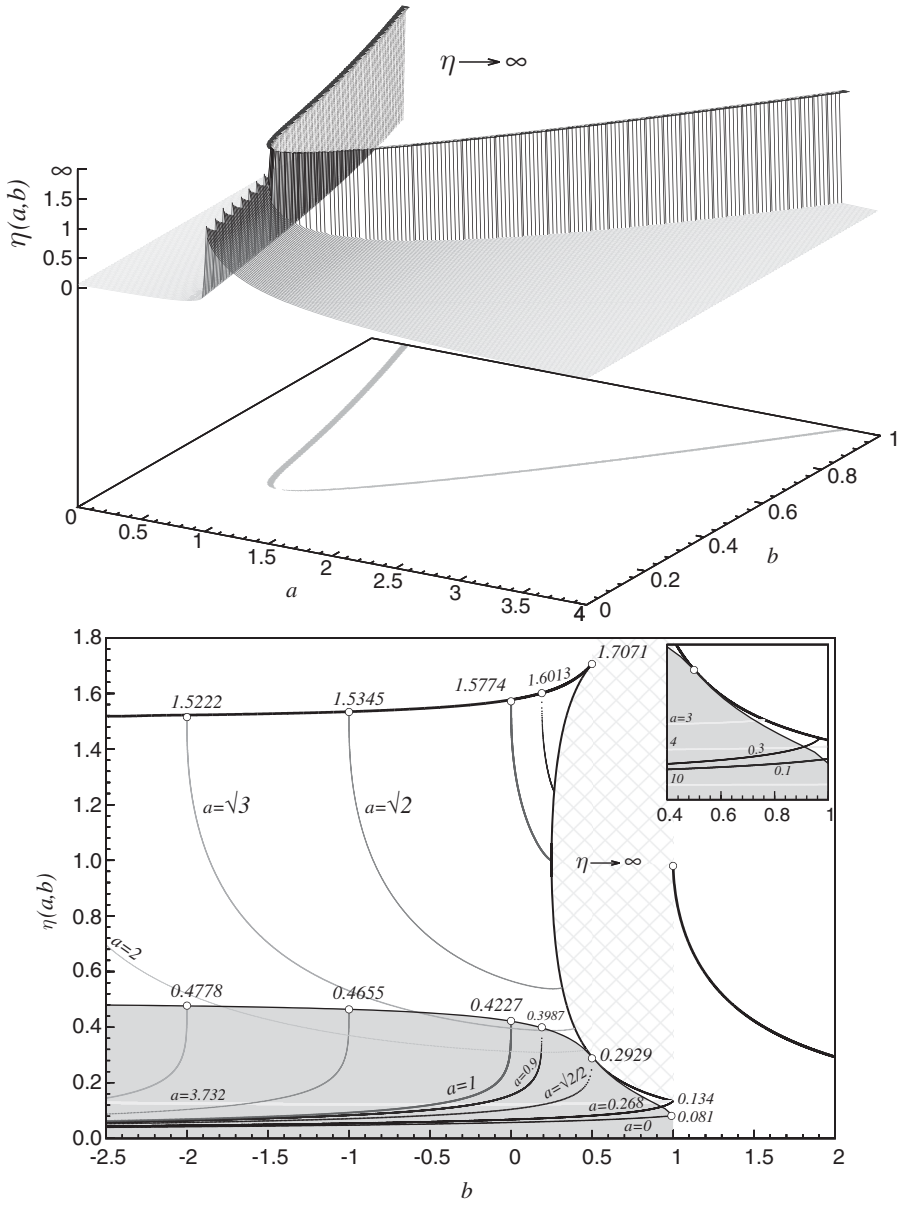

FIG. 25. The energetic efficiency $\eta(a,b)$ of the Keplerian accretion following the upper family circular geodesics is given depending on the spacetime dimensionless tidal charge parameter b and the spin parameter a. The 3D diagram reflects the position of the special class of the mining-unstable Kerr-Newman spacetimes of class IIIa in the plane of the spacetime parameters. Because of the complex character of the efficiency function, we also give the characteristic $a = \text{const}$ sections in the η-b plane.

$\lambda = L/E > 0$. In the third case, the Keplerian accretion efficiency (theoretically) approaches infinity. This effect occurs explicitly in the class IIIa Kerr-Newman spacetimes, as clearly demonstrated in Fig. 11. For this class, we have the tidal charge parameter $b \in (1/4, 1)$ and the dimensionless spin $a \in (2\sqrt{b} - \sqrt{b(4b-1)}, 2\sqrt{b} + \sqrt{b(4b-1)})$.

The Keplerian accretion efficiency is given for the upper family of circular geodesics in Fig. 25, and for the lower family circular orbits in Fig. 26. Because of its complexity, we represent the case of the upper family accretion regime by a 3D figure, with the addition of a figure representing the relevant sections $a = \text{const}$. In the case of the lower family accretion regime, the representative $a = \text{const}$ sections are sufficient to clearly demonstrate the character of the efficiency of the Keplerian accretion.

For the Keplerian accretion along the lower family circular geodesics, the situation is quite simple and the efficiency is always continuously matched between the naked singularity and the extreme black hole states. The efficiency of the lower family regime accretion for fixed dimensionless spin a of the braneworld Kerr-Newman spacetimes always decreases with a decreasing

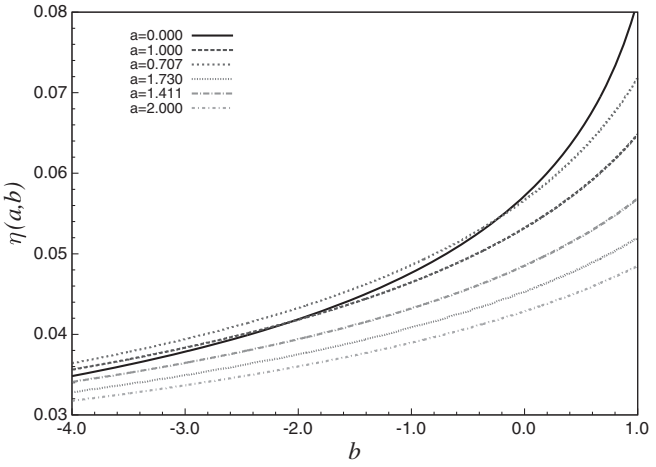

FIG. 26. Energy efficiency of the Keplerian accretion following the lower family circular geodesics is given depending on the spacetime dimensionless tidal charge parameter b for characteristic values of the spin parameter $a = \text{const}$.

tidal charge parameter b. Moreover, for a fixed tidal charge b, the efficiency decreases with an increasing spin a.

For understanding the upper family Keplerian accretion regime and its efficiency, the dependences $\eta(b, a = \text{const})$ are most instructive. They are governed by two crucial families of curves. First, the efficiency of the Keplerian accretion in the extreme braneworld KN black hole spacetimes and the related near-extreme braneworld KN naked singularity spacetimes are given by the relation

$$\eta_{\text{jump}}(b) = 1 \pm \frac{1}{\sqrt{4 - \frac{1}{1-b}}}, \tag{109}$$

where the plus sign corresponds to the efficiency in the near-extreme naked singularity spacetimes, while the minus sign corresponds to the related extreme black holes. Naturally, this formula is relevant in the interval of the tidal charge $b \in (-\infty, 0.5)$, i.e., up to the critical value of the tidal charge. Second, a crucial curve is given by the efficiency of the accretion in the limiting spacetimes governed by the boundary of class IIIa spacetimes, $\eta_{\text{mining}}(b, a_{\text{mining}\pm}(b))$, where $b \in (1/4, 1)$, and $a_{\text{mining}}(b) = 2\sqrt{b} \pm \sqrt{b(4b-1)}$.

The results can be summarized in the following way. For all of the braneworld spacetimes with the negative tidal charge parameter $b < 0$, and for those with positive charge parameter $0 \leq b \leq 1/2$, the large jump in efficiency in the transition between the naked singularity and the related extreme black hole state occurs. Such a jump was observed for the first time in the case of the transition between the Kerr naked singularity and the extreme Kerr black hole ($b = 0$), where $\eta \sim 1.57$ goes down to $\eta \sim 0.43$ [35]. For the braneworld KN extreme black holes (the related near-extreme naked singularities), the efficiency slightly increases (decreases) with negatively valued tidal charge increasing in its magnitude, so the efficiency jump slightly decreases from its maximal Kerr value. On the other hand, for $b \in (0, 1/2)$, the efficiency for the extreme black holes (the near-extreme naked singularities) decreases (increases), and the jump quickly increases—for $b = 1/2$, the efficiency jumps from $\eta \sim 1.707$ down to $\eta \sim 0.293$.

For the naked singularities with the tidal charge in the interval $1/4 < b < 1$ and the dimensionless spin in the interval $a \in (2\sqrt{b} - \sqrt{b(4b-1)},\ 2\sqrt{b} + \sqrt{b(4b-1)})$, the formally defined efficiency of the Keplerian accretion is unlimited. At the boundary of this region, the efficiency is given by the limit governed by the regular Keplerian accretion finished at the marginally stable orbit.

For the naked singularities with $b < 1/2$, the efficiency of the Keplerian accretion, starting at the near-extreme state and keeping spin $a = \text{const}$, decreases with an increasing tidal charge down to the curve $\eta_{\text{mining}}(b, a_{\text{mining}\pm}(b))$. A further increase of b causes an entrance to the region of unlimited efficiency. The curve $\eta(b, a = 1)$ starts at $b = 0$ and finishes at $b = 1/4$, giving the related efficiency $\eta = 1$. For a spin in the interval $1 > a > 1/\sqrt{2}$, the curves $\eta(b, a = 1)$ start at the extreme state and finish at the state with $0 < b < 1/2$ and efficiency $\eta > 1$. For a spin approaching $a = 1/\sqrt{2}$, the curve $\eta(b, a = \text{const})$ degenerates at the point with $b = 1/2$, and efficiency approaches $\eta \sim 1.707$. For higher values of spin, $a \in (1, 2 + \sqrt{3})$, the efficiency curves $\eta(b, a = \text{const})$ decrease to the curve $\eta_{\text{mining}}(b, a_{\text{mining}\pm}(b))$, with b increasing in the interval $b \in (1/4, 1)$ and the efficiency decreasing down to the limiting value of $\eta(b = 1, a = 2 + \sqrt{3}) \sim 0.134$.

For the tidal charge $b \in (1/2, 1)$, the efficiency of the Keplerian accretion at the transition between the extreme black hole and the related near-extreme naked singularity is continuously matched. The efficiency of $\eta \sim 0.134$ is reached for the Kerr-Newman spacetime with $b = 1$ and $a = 2 - \sqrt{3}$. For values of the spin in the interval of $a \in (2 - \sqrt{3}, 1/\sqrt{2})$, the transition of the function $\eta(b, a = \text{const})$ between the black hole and naked singularity states, obtained due to the increasing tidal charge b, is still continuous, and the curve $\eta_{\text{mining}}(b, a_{\text{mining}\pm}(b))$ is reached where $\eta < 0.293$.

With an increasing spin a, the efficiency of the Keplerian accretion decreases. It is interesting that, for naked singularities having a spin a higher than ~4.97 and an appropriately valued tidal charge b, the efficiency reaches values smaller than those corresponding to the Schwarzschild black holes ($\eta \sim 0.057$).

Note that the results of the Keplerian accretion analysis for the braneworld Kerr-Newman spacetimes can also be directly applied to the Keplerian accretion in the standard Kerr-Newman spacetimes, if we make the transformation $b \to Q^2$, where Q^2 represents the electric charge parameter of the Kerr-Newman background.

VIII. CONCLUSIONS

In this paper the circular geodesics of the braneworld Kerr-Newman black hole and naked singularity spacetimes have been studied, and classification of these spacetimes according to the character of the circular geodesic structure has been presented. The circular geodesics have been separated into two families—the lower family containing only the counterrotating circular geodesics and the upper family with corotating geodesics at a large distance, but a possible transformation to counterrotating geodesics in the vicinity of the naked singularity. It has been demonstrated that 14 different classes of the Kerr-Newman spacetimes can exist, mainly due to the properties of the upper family of circular geodesics. Implications of the geodesic structure to the Keplerian accretion have been given, and efficiency of the Keplerian accretion has been determined. The accretion efficiency is continuously matched between the naked singularity and extreme black hole spacetimes for the Keplerian accretion along the lower family circular geodesics. On the other hand, there is a strong discontinuity occurring in the transition between the naked singularities and the extreme black holes for the Keplerian accretion along the upper family circular geodesic, if the dimensionless spin of the Kerr-Newman spacetime is sufficiently high ($a > 1/\sqrt{2}$)—the energy efficiency of the Keplerian accretion is then substantially higher for the naked singularity spacetimes. The accretion efficiency could then go up to the value of $\eta \sim 1.707$ for Kerr-Newman near-extreme naked singularity spacetimes with $b \sim 1/2$ and $a \sim 1/\sqrt{2}$.

For the Keplerian accretion along the lower family circular geodesics, the inner edge of the disk always has to be located at the marginally stable circular geodesic corresponding to an inflection point of the effective potential of the motion, in accord with the scenario of the Keplerian accretion onto Kerr black holes and naked singularities.

It has been shown that the Keplerian accretion along the upper family geodesics can give three different scenarios. It can finish at the inner edge located at the marginally stable circular geodesic—this is the standard accretion scenario present in the black hole spacetimes. However, two other scenarios could occur in the naked singularity spacetimes. The inner edge of the Keplerian accretion could occur at $r = b$, which is the special limit on the existence of the circular geodesics. For $b > 1$ the efficiency of the upper family Keplerian accretion is independent of the naked singularity spin. The most interesting is the third scenario, related to the Kerr-Newman naked singularity spacetimes of class IIIa having an infinitely deep gravitational potential of the upper family Keplerian accretion. Then the inner edge of the Keplerian accretion could occur even at the stable photon circular geodesic, and the accretion efficiency could be formally unlimited, making such naked singularity spacetimes unstable relative to accretion mining.

The mining instability of the Kerr-Newman naked singularity spacetimes (or related superspinars) is a classical instability that could imply interesting consequences, which we plan to study in the future. Nevertheless, it is clear that the mining instability has to at least be restricted by the validity of the test particle approximation used in this paper for the Keplerian accretion.

The other classical instability, related to the conversion of Kerr naked singularities to extreme black holes due to the Keplerian accretion [36], has to be treated in future work, but this instability necessarily has a much more complex character in the Kerr-Newman naked singularity spacetimes in comparison to the relatively simple Kerr case, due to the complexities related to the mining instability and the influence of the tidal charge.

Interesting phenomena could be expected in the mining-unstable Kerr-Newman spacetimes (class IIIa) even if it will represent an astrophysically more acceptable concept of the Kerr-Newman superspinar, with the inner boundary of the Kerr-Newman spacetime located at least at the outer boundary of the causality violation region [37,40,41]. We can expect observations of extremely high energy coming out of collisions in the vicinity of such a superspinar, enabled by the nonexistence of the event horizon and the fast rotation of the superspinar or, inversely, the strong magnification of the incoming radiation [42,66]. We could expect a hot doughnut-shaped configuration of accreting matter surrounding the superspinar, as discussed in [60].

ACKNOWLEDGMENTS

Z. S. and M. B. have been supported by the Albert Einstein Centre for Gravitation and Astrophysics, financed by Czech Science Agency Grant No. 14-37086G and by Silesian University at Opava Grant No. SGS/14/2016. M. B. thanks Petr Slaný for several discussions.

[1] P. Hořava and E. Witten, Eleven-dimensional supergravity on a manifold with boundary, Nucl. Phys. **B475**, 94 (1996).
[2] P. Hořava and E. Witten, Heterotic and Type I string dynamics from eleven dimensions, Nucl. Phys. **B460**, 506 (1996).
[3] N. Arkani-Hamed, S. Dimopoulos, and G. Dvali, The hierarchy problem and new dimensions at a millimeter, Phys. Lett. B **429**, 263 (1998).
[4] L. Randall and R. Sundrum, An Alternative to Compactification, Phys. Rev. Lett. **83**, 4690 (1999).
[5] S. Dimopoulos and G. Landsberg, Black Holes at the Large Hadron Collider, Phys. Rev. Lett. **87**, 161602 (2001).
[6] T. Shiromizu, K.-I. Maeda, and M. Sasaki, The Einstein equations on the 3-brane world, Phys. Rev. D **62**, 024012 (2000).
[7] C. Germani and R. Maartens, Stars in the braneworld, Phys. Rev. D **64**, 124010 (2001).
[8] J. Hladík and Z. Stuchlík, Photon and neutrino redshift in the field of braneworld compact stars, J. Cosmol. Astropart. Phys. 07 (2011) 012.
[9] Z. Stuchlík, J. Hladík, and M. Urbanec, Neutrino trapping in braneworld extremely compact stars, Gen. Relativ. Gravit. **43**, 3163 (2011).
[10] N. Dadhich, R. Maartens, P. Papadopoulos, and V. Rezania, Black holes on the brane, Phys. Lett. B **487**, 1 (2000).
[11] A. N. Aliev and A. E. Gümrükçüoğlu, Charged rotating black holes on a 3-brane, Phys. Rev. D **71**, 104027 (2005).
[12] C. W. Misner, K. S. Thorne, and J. A. Wheeler, *Gravitation* (W.H. Freeman, New York, 1973).
[13] Z. Stuchlík and M. Calvani, Null geodesics in black hole metrics with non-zero cosmological constant, Gen. Relativ. Gravit. **23**, 507 (1991).
[14] Z. Stuchlík and S. Hledík, Equatorial photon motion in the Kerr-Newman spacetimes with a non-zero cosmological constant, Classical Quantum Gravity **17**, 4541 (2000).
[15] Z. Stuchlík and S. Hledík, Properties of the Reissner-Nordström spacetimes with a nonzero cosmological constant, Acta Phys. Slovaca **52**, 363 (2002).
[16] D. Pugliese, H. Quevedo, and R. Ruffini, Equatorial circular motion in Kerr spacetime, Phys. Rev. D **84**, 044030 (2011).
[17] D. Pugliese, H. Quevedo, and R. Ruffini, Equatorial circular orbits of neutral test particles in the Kerr-Newman spacetime, Phys. Rev. D **88**, 024042 (2013).
[18] J. Schee and Z. Stuchlík, Profiles of emission lines generated by rings orbiting braneworld Kerr black holes, Gen. Relativ. Gravit. **41**, 1795 (2009).
[19] J. Schee and Z. Stuchlík, Optical phenomena in the field of braneworld Kerr black holes, Int. J. Mod. Phys. D **18**, 983 (2009).
[20] A. Y. Bin-Nun, Relativistic images in Randall-Sundrum II braneworld lensing, Phys. Rev. D **81**, 123011 (2010).
[21] E. F. Eiroa, Braneworld black hole gravitational lens: Strong field limit analysis, Phys. Rev. D **71**, 083010 (2005).
[22] F. Atamurotov, A. Abdujabbarov, and B. Ahmedov, Shadow of rotating non-Kerr black hole, Phys. Rev. D **88**, 064004 (2013).
[23] J. Jiang, C. Bambi, and J. F. Steiner, Testing the Kerr nature of black hole candidates using iron line reverberation mapping in the Cardoso-Pani-Rico framework, Phys. Rev. D **93**, 123008 (2016).
[24] D. Liu, Z. Li, and C. Bambi, Testing a class of non-Kerr metrics with hot spots orbiting SgrA*, J. Cosmol. Astropart. Phys. 02 (2015) 020.
[25] Z. Li, L. Kong, and C. Bambi, Testing the nature of the supermassive black hole candidate in SgrA* with light curves and images of hot spots, Astrophys. J. **787**, 152 (2014).
[26] C. G. Böhmer, T. Harko, and F. S. N. Lobo, Solar system tests of brane world models, Classical Quantum Gravity **25**, 045015 (2008).
[27] A. Kotrlová, Z. Stuchlík, and G. Török, Quasiperiodic oscillations in a strong gravitational field around neutron stars testing braneworld models, Classical Quantum Gravity **25**, 225016 (2008).
[28] Z. Stuchlík and A. Kotrlová, Orbital resonances in discs around braneworld Kerr black holes, Gen. Relativ. Gravit. **41**, 1305 (2009).
[29] A. N. Aliev and P. Talazan, Gravitational effects of rotating braneworld black holes, Phys. Rev. D **80**, 044023 (2009).
[30] A. Abdujabbarov and B. Ahmedov, Test particle motion around a black hole in a braneworld, Phys. Rev. D **81**, 044022 (2010).
[31] O. G. Rahimov, A. A. Abdujabbarov, and B. J. Ahmedov, Magnetized particle capture cross section for braneworld black hole, Astrophys. Space Sci. **335**, 499 (2011).
[32] V. S. Morozova and B. J. Ahmedov, Electromagnetic fields of slowly rotating compact magnetized stars in braneworld, Astrophys. Space Sci. **333**, 133 (2011).
[33] S. R. Shaymatov, B. J. Ahmedov, and A. A. Abdujabbarov, Particle acceleration near a rotating black hole in a Randall-Sundrum brane with a cosmological constant, Phys. Rev. D **88**, 024016 (2013).
[34] F. de Felice, Repulsive phenomena and energy emission in the field of a naked singularity, Astron. Astrophys. **34**, 15 (1974).
[35] Z. Stuchlík, Equatorial circular orbits and the motion of the shell of dust in the field of a rotating naked singularity, Bull. Astron. Inst. Czech. **31**, 129 (1980).
[36] Z. Stuchlík, S. Hledík, and K. Truparová, Evolution of Kerr superspinars due to accretion counterrotating thin discs, Classical Quantum Gravity **28**, 155017 (2011).
[37] Z. Stuchlík and J. Schee, Observational phenomena related to primordial Kerr superspinars, Classical Quantum Gravity **29**, 065002 (2012).
[38] R. C. Henry, Kretschmann scalar for a Kerr-Newman black hole, Astrophys. J. **535**, 350 (2000).
[39] B. Carter, in *Black Holes (Les Astres Occlus)*, edited by C. Dewitt and B. S. Dewitt (Gordon and Breach, New York, 1973), p. 57.
[40] E. G. Gimon and P. Hořava, Astrophysical violations of the Kerr bound as a possible signature of string theory, Phys. Lett. B **672**, 299 (2009).
[41] Z. Stuchlík and J. Schee, Appearance of Keplerian discs orbiting Kerr superspinars, Classical Quantum Gravity **27**, 215017 (2010).
[42] Z. Stuchlík and J. Schee, Ultra-high-energy collisions in the superspinning Kerr geometry, Classical Quantum Gravity **30**, 075012 (2013).
[43] J. M. Bardeen, W. H. Press, and S. A. Teukolsky, Rotating black holes: Locally nonrotating frames, energy extraction, and scalar synchrotron radiation, Astrophys. J. **178**, 347 (1972).

[44] Z. Stuchlík, J. Bičák, and V. Bálek, The shell of incoherent charged matter falling onto a charged rotating black hole, Gen. Relativ. Gravit. **31**, 53 (1999).
[45] B. Carter, Global structure of the Kerr family of gravitational fields, Phys. Rev. **174**, 1559 (1968).
[46] G. V. Kraniotis, Frame dragging and bending of light in Kerr and Kerr (anti–)de Sitter spacetimes, Classical Quantum Gravity **22**, 4391 (2005).
[47] G. V. Kraniotis, Periapsis and gravitomagnetic precessions of stellar orbits in Kerr and Kerr–de Sitter black hole spacetimes, Classical Quantum Gravity **24**, 1775 (2007).
[48] Z. Stuchlík, The motion of test particles in black-hole backgrounds with non-zero cosmological constant, Bull. Astron. Inst. Czech. **34**, 129 (1983).
[49] Z. Stuchlík and S. Hledík, Some properties of the Schwarzschild–de Sitter and Schwarzschild–anti-de Sitter spacetimes, Phys. Rev. D **60**, 044006 (1999).
[50] G. V. Kraniotis, Gravitational lensing and frame dragging of light in the Kerr-Newman and the Kerr-Newman (anti–)de Sitter black hole spacetimes, Gen. Relativ. Gravit. **46**, 1818 (2014).
[51] Z. Stuchlík, Evolution of Kerr naked singularities, Bull. Astron. Inst. Czech. **32**, 68 (1981).
[52] V. Bálek, J. Bičák, and Z. Stuchlík, The motion of the charged particles in the field of rotating charged black holes and naked singularities. II. The motion in the equatorial plane, Bull. Astron. Inst. Czech. **40**, 133 (1989).
[53] Z. Kovács and T. Harko, Can accretion disk properties observationally distinguish black holes from naked singularities?, Phys. Rev. D **82**, 124047 (2010).
[54] N. Dadhich and P. P. Kale, Equatorial circular geodesics in the Kerr-Newman geometry, J. Math. Phys. (N.Y.) **18**, 1727 (1977).
[55] I. D. Novikov and K. S. Thorne, in *Black Holes (Les Astres Occlus)*, edited by C. Dewitt and B. S. Dewitt (Gordon and Breach, New York, 1973), p. 343.
[56] D. N. Page and K. S. Thorne, Disk-accretion onto a black hole. Time-averaged structure of accretion disk, Astrophys. J. **191**, 499 (1974).
[57] J. Bičák, Z. Stuchlík, and V. Bálek, The motion of charged particles in the field of rotating charged black holes and naked singularities, Bull. Astron. Inst. Czech. **40**, 65 (1989).
[58] J. M. Bardeen, in *Black Holes (Les Astres Occlus)*, edited by C. Dewitt and B. S. Dewitt (Gordon and Breach, New York, 1973), p. 215.
[59] R. Ruffini, in *Black Holes (Les Astres Occlus)*, edited by C. Dewitt and B. S. Dewitt (Gordon and Breach, New York, 1973), p. 451.
[60] Z. Stuchlík and J. Schee, Optical effects related to Keplerian discs orbiting Kehagias-Sfetsos naked singularities, Classical Quantum Gravity **31**, 195013 (2014).
[61] J. Bičák and Z. Stuchlík, On the latitudinal and radial motion in the field of a rotating black hole, Bull. Astron. Inst. Czech. **27**, 129 (1976).
[62] See, for example, Refs. [15,63].
[63] M. Favata, Conservative corrections to the innermost stable circular orbit (ISCO) of a Kerr black hole: A new gauge-invariant post-Newtonian ISCO condition, and the ISCO shift due to test-particle spin and the gravitational self-force, Phys. Rev. D **83**, 024028 (2011).
[64] Interestingly, the Keplerian efficiency relation for the lower family of geodetics is much more complex and depends on the spin parameter *a*.
[65] Z. Stuchlík, Null geodesics in the Kerr-Newman metric, Bull. Astron. Inst. Czech. **32**, 366 (1981).
[66] Z. Stuchlík, J. Schee, and A. Abdujabbarov, Ultra-high-energy collisions of particles in the field of near-extreme Kehagias-Sfetsos naked singularities and their appearance to distant observers, Phys. Rev. D **89**, 104048 (2014).
[67] Z. Stuchlík and J. Schee, Circular geodesic of Bardeen and Ayon-Beato-Garcia regular black-hole and no-horizon spacetimes, Int. J. Mod. Phys. D **24**, 1550020 (2015).
[68] J. Schee and Z. Stuchlík, Gravitational lensing and ghost images in the regular Bardeen no-horizon spacetimes, J. Cosmol. Astropart. Phys. 06 (2015) 048.
[69] Formally, the same results relevant to Kerr-Newman spacetime can be found in [70].
[70] A. N. Aliev and D. V. Galtsov, Radiation from relativistic particles in nongeodesic motion in a strong gravitational field, Gen. Relativ. Gravit. **13**, 899 (1981).